37

N63-10332

CODE 1 CODE 1

Technical Report No. 32-269

Heat and Momentum Transfer in Smooth and Rough Tubes at Various Prandtl Numbers

Duane F. Dipprey
Rolf H. Sabersky

jpl
JET PROPULSION LABORATORY
CALIFORNIA INSTITUTE OF TECHNOLOGY
PASADENA, CALIFORNIA

June 6, 1962

NATIONAL AERONAUTICS AND SPACE ADMINISTRATION
CONTRACT NO. NAS 7-100

Technical Report No. 32-269

Heat and Momentum Transfer in Smooth and Rough Tubes at Various Prandtl Numbers

Duane F. Dipprey
Rolf H. Sabersky

D. R. Bartz, Chief
Propulsion Research Section

JET PROPULSION LABORATORY
CALIFORNIA INSTITUTE OF TECHNOLOGY
PASADENA, CALIFORNIA

June 6, 1962

CONTENTS

FIGURES

ABSTRACT

Results are presented from an experimental investigation of the relation between heat transfer and friction in smooth and rough tubes. Three rough tubes and one smooth tube were formed from electroplated nickel. The rough tubes contained a close-packed, granular type of surface with roughness-height-to-diameter ratios ranging from 0.0024 to 0.049. Measurements of the heat transfer coefficients (C_H) and the friction coefficients (C_F) were obtained with distilled water flowing through the electrically heated tubes. A Prandtl number range of 1.20 to 5.94 was investigated by adjusting the bulk temperature of the water. Results were obtained for Reynolds numbers from 6×10^4 to 5×10^5 and from 1.4×10^4 to 1.2×10^5 at the lowest and highest Prandtl number, respectively.

A similarity rule for heat transfer was used to correlate, interpret, and extend the experimental results. The results were compared with previously existing results, both theoretical and experimental. Increases in C_H due to roughness of as high as 270% were obtained. These increases were, in general, accompanied by even larger increases in C_F. An exception to this general behavior occurs at high Prandtl number in the region of transition between the "smooth" and "fully rough" C_F characteristic.

I. INTRODUCTION

The role played by rough surfaces in fluid mechanics and heat transfer has been of interest for a long time. On the one hand this interest has been for practical reasons because of the increase in friction and heat transfer rate associated with rough surfaces. On the other hand the effect of roughness on the flow profiles and the exchange properties of the flow have posed an intriguing problem for students of basic fluid mechanics.

A most complete study of the effect of roughness on friction and velocity distribution, was completed in 1933 by Nikuradse (Ref. 1) who conducted the now-classical series of experiments with pipes roughened by sand grains. In contrast to this very thorough and complete experimental work, the study of the effect of roughness on heat transfer has received relatively little attention. A partial explanation for this lack may lie in the difficulties involved in obtaining highly accurate heat transfer measurements and in the fact that for a complete study of the heat transfer phenomena the influence of the Prandtl number has to be studied in addition to that of the flow parameters.

One of the first studies of heat transfer in rough tubes was conducted by Cope (Ref. 2) in 1941, and a very thorough study involving largely two dimensional roughness elements and using air as the working fluid was published by Nunner (Ref. 3) in 1958. The purpose of the

present study was to provide a set of experimental data on the friction as well as heat transfer characteristics of rough surfaces for a relatively wide range of Reynolds numbers, roughness ratios, and Prandtl numbers. It was hoped that a set of data of this sort would be useful directly for some design purposes and that it may also form a basis of comparison for certain hypotheses that can be offered as an explanation for the action of roughnesses.

Considerable thought was given to the selection of the roughness type to be used in the present work. Two-dimensional roughnesses such as could be formed by concentric rings or by screw threads, three-dimensional roughnesses formed by spherical segments or sand grains, and naturally rough surfaces as well as several others were most carefully considered. It was finally decided to conduct the experiments with surfaces having a close-packed sand-grain-type roughness. Not the least factor in this decision was the existence of Nikuradse's work on friction and velocity distribution which was done with similar surfaces. It was thought that the use of this same type of surface would permit the present heat transfer results to be regarded as an extension of Nikuradse's work on friction and would thus prove most serviceable in view of the large amount of thought which has been given to the data of Nikuradse. Furthermore, the sand grain roughness simulates natural roughness to some extent because of its three dimensional nature and of the random shape of the roughness elements. Lastly, by selecting a narrow grain size distribution, various roughness sizes were obtained. With this selection, of course, the random size distribution characteristics of a natural roughness is lost. This compromise was, however, deemed allowable, and a sand-grain-type roughness was selected as a consequence.

II. EXPERIMENTAL PROCEDURES

The experiments[1] were conducted with distilled water flowing upward through a nominally 0.4-in.-diameter tube which was heated by the passage of alternating-current electricity through the tube walls. Friction coefficients were determined from fluid flow rate and pressure drop measurements, and the heat transfer coefficients were determined from measurements of heating power, outside tube-wall temperature, and fluid temperature. Fully established conditions were approximated by providing 45 diameters of hydrodynamic entrance length followed by 38 diameters of thermal entrance length ahead of the station at which the heat transfer coefficient was to be measured. The effects of radial temperature gradients accompanying finite heat flux values were eliminated by extrapolating the Stanton number (C_H) results, from tests with various wall-to-fluid temperature differences, to the zero temperature difference condition. Prandtl number variations from 1.20 to 5.94, were achieved by setting the water bulk temperature at selected values from 80 to 290°F. The Reynolds number was independently varied in the range from 1.4×10^4 to 5.2×10^5 by adjusting the water flow rate.

The facility used in the experiments is depicted schematically in Fig. 1. The water was pumped, by nitrogen gas pressure, from the reservoir tank, through the test section and into the receiver tank. Settings of the gas regulators and the throttle valve controlled the flow. The flow rate was measured by means of a calibrated venturi meter and bellows-type differential pressure gages. Similar gages were used to measure test section pressure-drop. The heating power for the tube was supplied through a 100 KVA, variable-primary transformer. This power was determined both by measurements of the input electrical power and by measurement of the temperature rise of the fluid passing the test section.

The three rough tubes used for the experiments were produced by electroplating nickel over mandrels coated with closely graded sand grains. The mandrels were subsequently dissolved with chemicals leaving a pure nickel shell which served as the test tube. Before plating, the surfaces of the sanded mandrels were partially filled with lacquer such that the nickel casts of the surfaces gave the general appearance of an array of close-packed sand grains (cf. Fig. 2). A smooth tube was also produced by the same method using a smooth mandrel. The tube wall material was found to be of high purity, free of inclusions and uniform throughout. In the construction of the test section, shown in Fig. 3, each of the nickel test tubes (nominally 36 in. long, 0.4 in. in diameter, and 0.020 in. thick) was fitted with copper electrodes, pressure

[1]Reference 4 contains a more detailed discussion of the experiments.

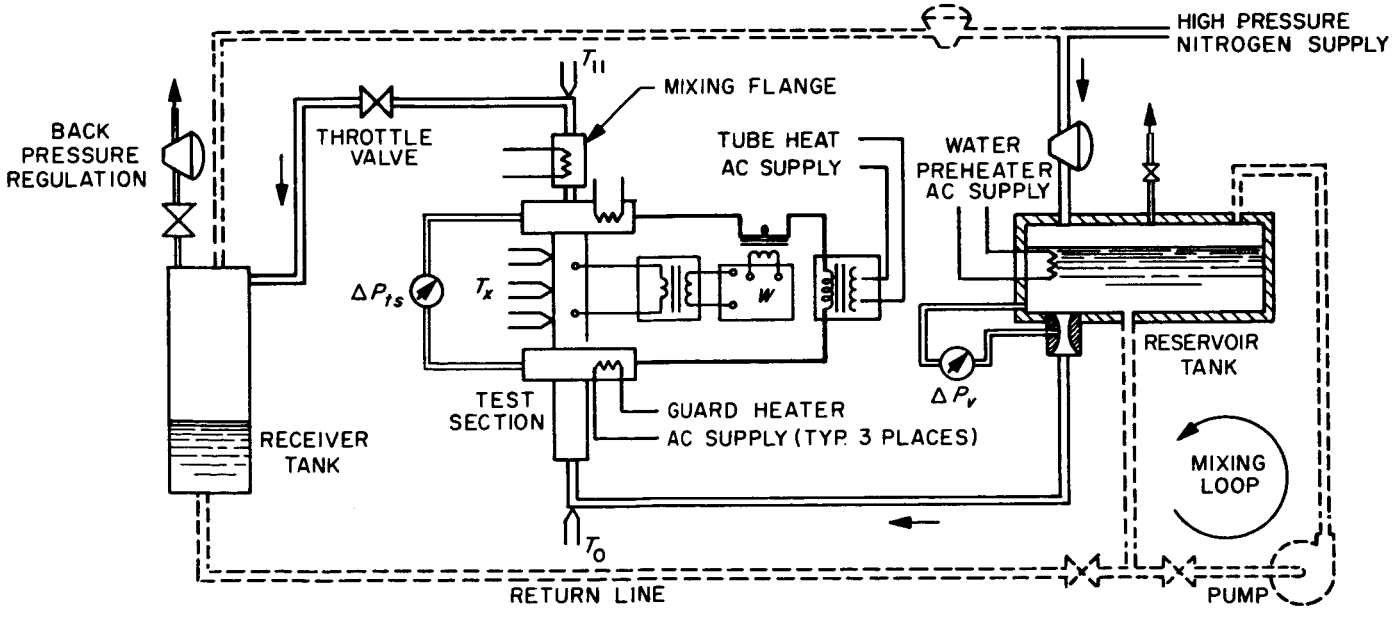

Fig. 1. Simplified test facility schematic

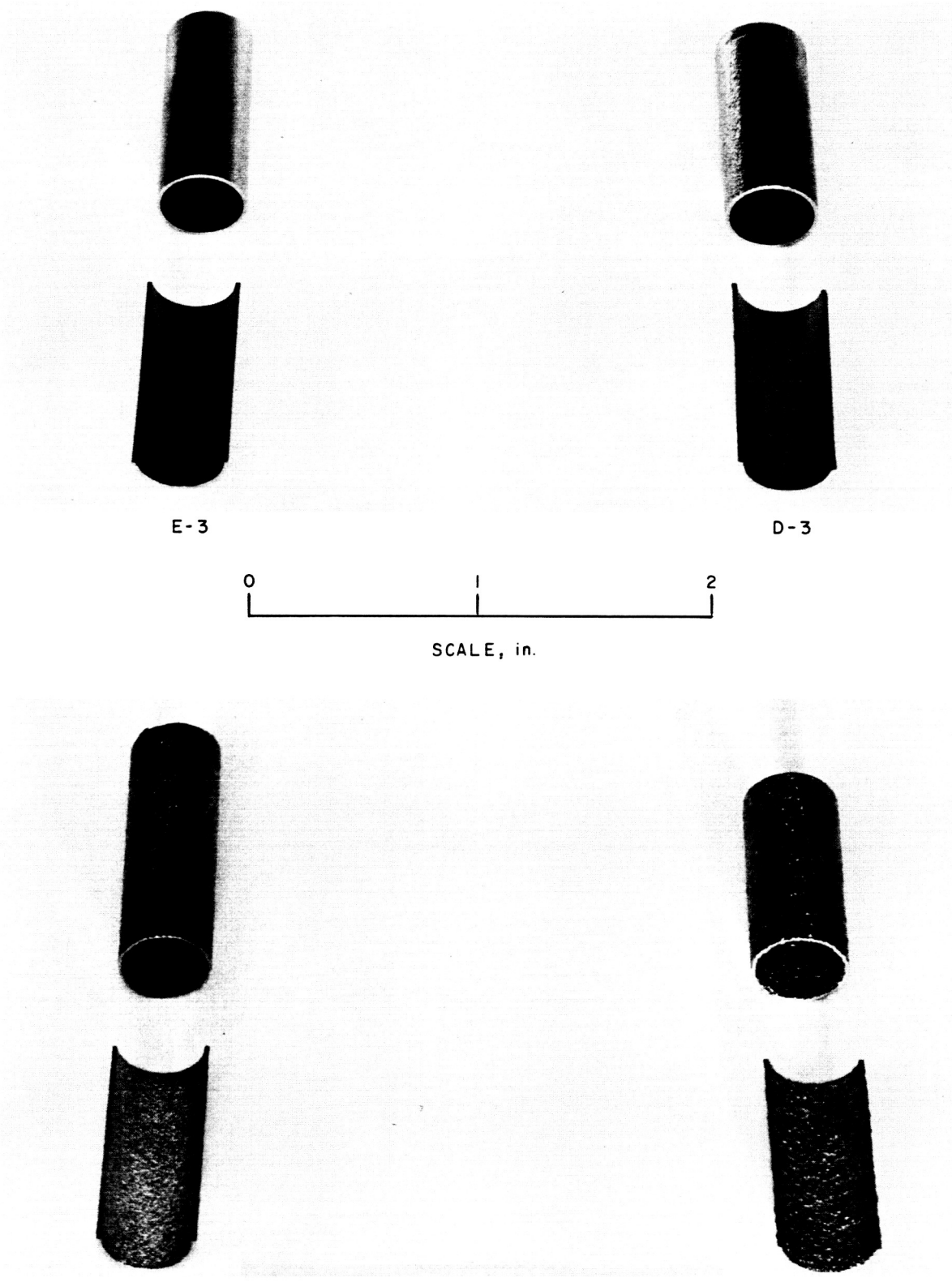

Fig. 2. Tube samples

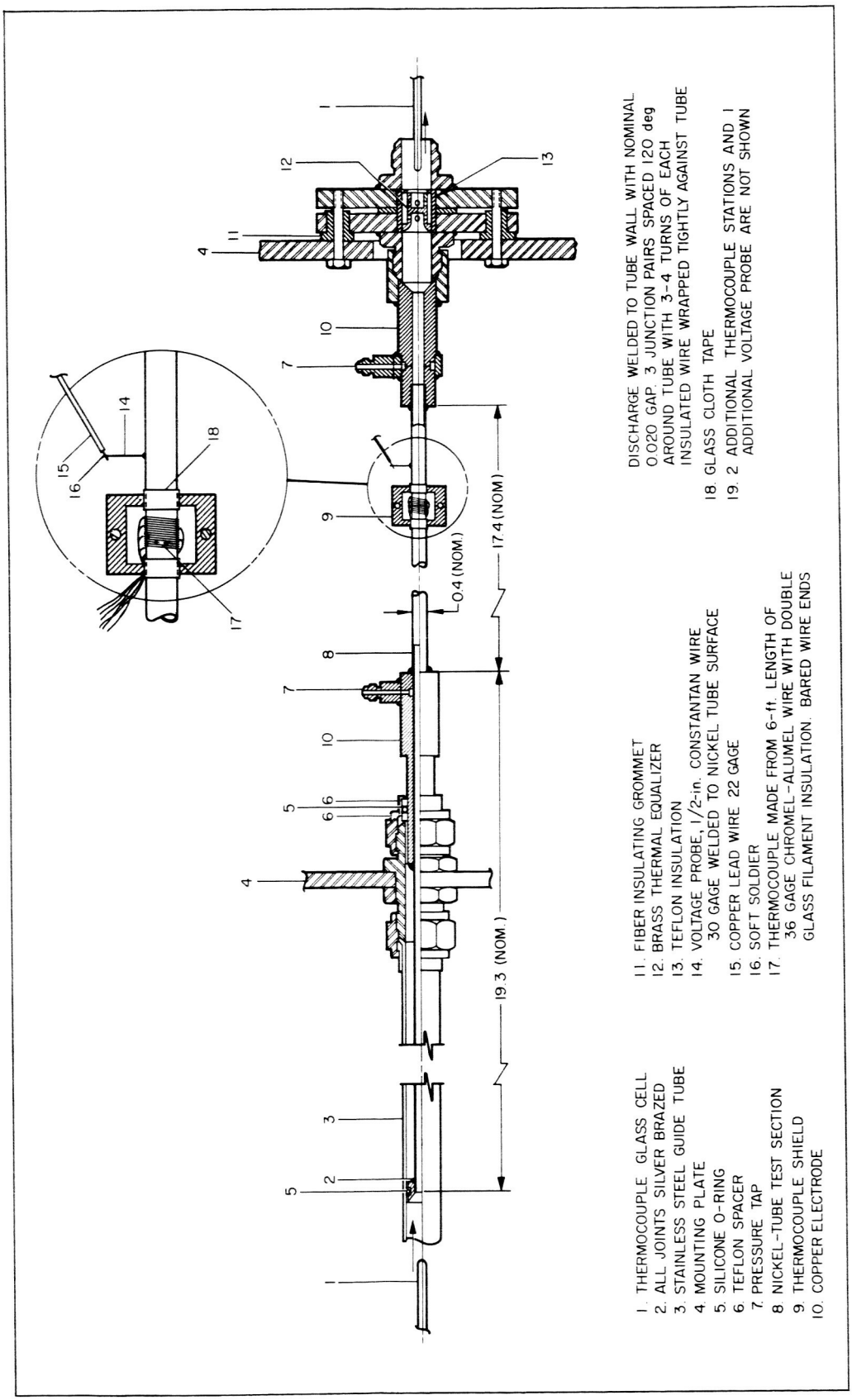

Fig. 3. Test section assembly

taps, voltage taps, and a set of nine outside wall thermocouples. The respective tube dimensions and the locations of the various measurements stations are listed in Table 1. In this table the inside diameter, D, of the rough tubes is defined on the basis of the volume contained in an incremental length of tube. The thickness, t_7, which is used in the determination of the tube wall temperature drop is an effective thickness determined from measurements of the electrical resistance of the tubes.

The calorimetric power determinations were facilitated by the mixing flange and two immersion-type thermocouples fused in glass cells. The latter were used to monitor the inlet and outlet bulk water temperatures. Outputs from all of the thermocouples, including those mounted on the tube wall, were measured with a hand balance potentiometer-galvanometer. Switches were provided to permit measurement of the emf difference between any of the thermocouples and the outlet water thermocouple. In the case of the rough tubes, the static pressure taps were placed in short smooth sections, the center tap area being formed in the nickel tube and the exit tap area being machined in the exit electrode. The two voltage probes on the tube walls were used to measure local power input in the region of the downstream thermocouple station.

Since it was desired to obtain data with accuracies sufficient for testing theoretical deductions, considerable redundancy and extensive calibrations were employed in the measurements. The differential pressure recording gages were calibrated *in situ* against manometers. The metering venturi was calibrated, as installed in the system, against a weighed discharge. The electrical power meters were calibrated against standard instruments and redundant measurements of power input were provided in each test. The glass-cell, immersion thermocouples were calibrated against mercury-in-glass thermometers in a controlled furnace. A series of calibration tests at each of the nominal combinations of water flow rate and temperature was performed on each tube. These tests were carried out in the same way as the heat transfer test except that no heating power was applied. The resulting data were used to provide the isothermal friction vs Reynolds number characteristics of each tube and to calibrate the tube-wall thermocouples against the immersion

Table 1. Tube dimensions

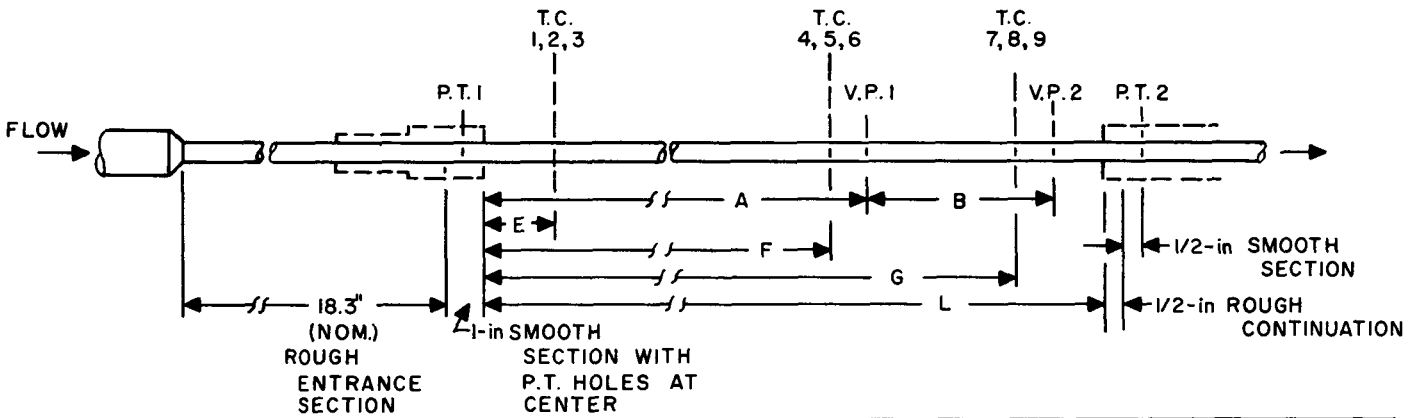

	ALL DIMENSIONS IN INCHES										
TUBE	D	L	t_7	d_{sg}	ϵ_s	ϵ_s/D	A	B	E	F	G
E-3	0.377	17.40	0.0201	—	—	—	12.38	3.65	2.18	10.17	15.14
D-3	0.384	17.39	0.0226	0.0032	0.00092	0.0024	11.04	5.02	2.13	10.15	15.12
C-9	0.393	17.39	0.0176	0.0075	0.0054	0.0138	10.99	5.03	2.18	10.17	15.14
A-4	0.399	17.41	0.0187	0.0150	0.0195	0.0488	11.09	5.01	2.14	10.12	15.12

NOTES

P.T. PRESSURE TAP
V.P. VOLTAGE PROBE
T.C. THERMOCOUPLE
d_{sg} DIAMETER OF MANDREL SAND GRAINS
t_7 WALL THICKNESS AT T.C. STATION 7
E, F, G STATION OF T.C. 2, 5, 8, RESPECTIVELY
OTHER T.C.'S ~ ±0.15-in. FROM THESE LOCATIONS

thermocouples. These calibrations also provided corrections for secondary effects such as heat exchange at the electrodes.

By using the force balance equation for fully established flow, one obtains an expression for the friction factor used in the data reduction,

$$C_F = \frac{\pi^2 D^5 \rho \Delta P_{TS}}{32 w^2} \quad (1)$$

Small corrections were allowed for the pressure-drop of the smooth sections adjoining the pressure taps. The estimated error limits for the friction factor determinations vary from ±2.5% for the smooth tube to ±4.2% for the roughest tube (95% confidence coefficient).

The dimensionless heat transfer coefficient (Stanton number) is defined herein as

$$C_H \equiv \frac{q_0}{\rho u_m c_p \Delta T_f} \quad (2)$$

In the data reduction, the heat flux at the inner wall (q_0) was computed from measurement of the power generated in the tube and the dimensions of the test section. The wall-to-bulk-fluid temperature difference (ΔT_f) was obtained by adjusting the measured temperature difference, between the tube outer wall and the mixed fluid at the exit, to account for the temperature drop in the wall and the temperature rise of the fluid between the wall thermocouple station and the exit. The wall temperature drop was deduced from the heat flux, the tube geometry, the thermal conductivity and the electrical resistivity of the tube material. The use of pure nickel for the tubes made possible the use of existing experimental information on the material properties. An integration of the heat addition in the region between the wall thermocouple and the exit permitted computation of the temperature rise of the fluid passing this region. For reducing the heat transfer data to obtain local values of the heat transfer coefficient, the Reynolds number and the Prandtl number, correction factors were developed and applied which accounted for the effects of longitudinal variations in tube wall thickness and wall temperature. These variations cause a small, monotonic variation in heat flux with longitudinal station.

Tests at three different heat flux values were performed for each of the nominal combinations of water bulk temperature and flow rate, i.e., of Reynolds number and Prandtl number. To obtain the reported isothermal heat transfer coefficients, the data from each test were first adjusted to correspond to the nominal local Reynolds and Prandtl number conditions. The adjusted heat transfer coefficients (C_H) were then plotted against wall-to-mixed-fluid temperature difference (ΔT_f). An extrapolation of the straight line best approximating the three points provided an intercept with the ordinate ($\Delta T_f = 0$). This intercept was taken to represent the desired isothermal C_H value. In the case of the smooth tube, the observed sensitivity of heat transfer coefficients to variations in ΔT_f was found to be consistent with previously existing information (Ref. 5).

For each test, the average of the three, circumferentially displaced, measurements of heat transfer coefficient determined for each of the three thermocouple stations was plotted as a function of longitudinal station. In general, these plots showed very little difference between the heat transfer coefficients for the last two stations, at 26 and 40 diameters from the start of heating respectively. This implies that the desired conditions of hydrodynamically and thermally fully established flow were attained. For certain test conditions, the data obtained with the smooth tube and the smoothest of the rough tubes indicated that the C_H values at the 40 diameter point were slightly less than at 26 diameters.

The effects of spatial variations in liquid-side heat transfer film conductance, electric current density in the wall, and temperature-drop through the wall add to the uncertainty of the final results. This uncertainty increases with the size of the roughness elements. These effects, taken together with the previously mentioned uncertainties in the degree to which the flow is fully established and the possible errors in the instrument measurements, were combined to obtain the uncertainty limits of the final heat transfer results. The combined uncertainties in the reported heat transfer coefficients are less than ±5% (95% confidence coefficient) for most of the test conditions reported. For a few combinations of tube roughness, Prandtl number and Reynolds number, however, the value may reach ±7%. Of these uncertainties, less than ±2% is attributed to instrumentation and reading errors.

A deviation from the above uncertainty limits occurs in the case of the smoothest of the rough tubes (tube designation, D-3) operating at high Reynolds numbers. Relatively large circumferential variations in heat transfer coefficient were observed in this case making it necessary to degrade the resulting data to uncertainty limits of as large as ±17%. In the low Reynolds number region, wherein the friction characteristics of the D-3 tube were similar to that of a smooth tube, the circumferential C_H

variations did not appear. This observation contributes to the conclusion (Ref. 4) that differences in roughness height on different sides of the tube are responsible for the variations observed at high Reynolds number. This explanation is particularly plausible since the average physical height of the roughness elements in this tube is only approximately 0.001 in. so that large percentage variations could easily be incurred.

III. RESULTS FOR THE SMOOTH TUBE

Experiments were first carried out with a smooth tube. This work was performed for a dual purpose: first, to compare the present results with those of previous experimenters, thereby creating a general basis for evaluating the experimental methods employed, and secondly to establish a reference for the results obtained with the rough tubes.

As seen in Fig. 4, the friction coefficient for the smooth tube matches the data obtained by Nikuradse within less than $\pm 2\%$ (which is within the limits of experimental accuracy) from the lowest Reynolds number at which tests were conducted ($Re = 25{,}000$) to a Reynolds number of 300,000. The experimental range extended to Re values of about 500,000, but beyond 300,000 the surface finish of the so-called smooth tube was sufficiently coarse to cause a slight variation from the reference curve. The experiments showed, however, that up to a $Re = 300{,}000$ the tube fulfilled perfectly the conditions of a hydraulically smooth one.

The results for the heat transfer coefficient were compared with the data published by Eagle and Ferguson (Ref. 6) and Allen (Ref. 5); both of the referenced experiments are believed to have been conducted with extreme care. The variation of C_H vs Re at a given Pr was examined first. As the various experiments were conducted at different Pr, slight extrapolations were required to reduce the data to correspond to a single Prandtl number. The value of $Pr = 8$ was selected for this purpose as it required the least extrapolation. The subsequent comparison showed that the data of the three sets did not deviate

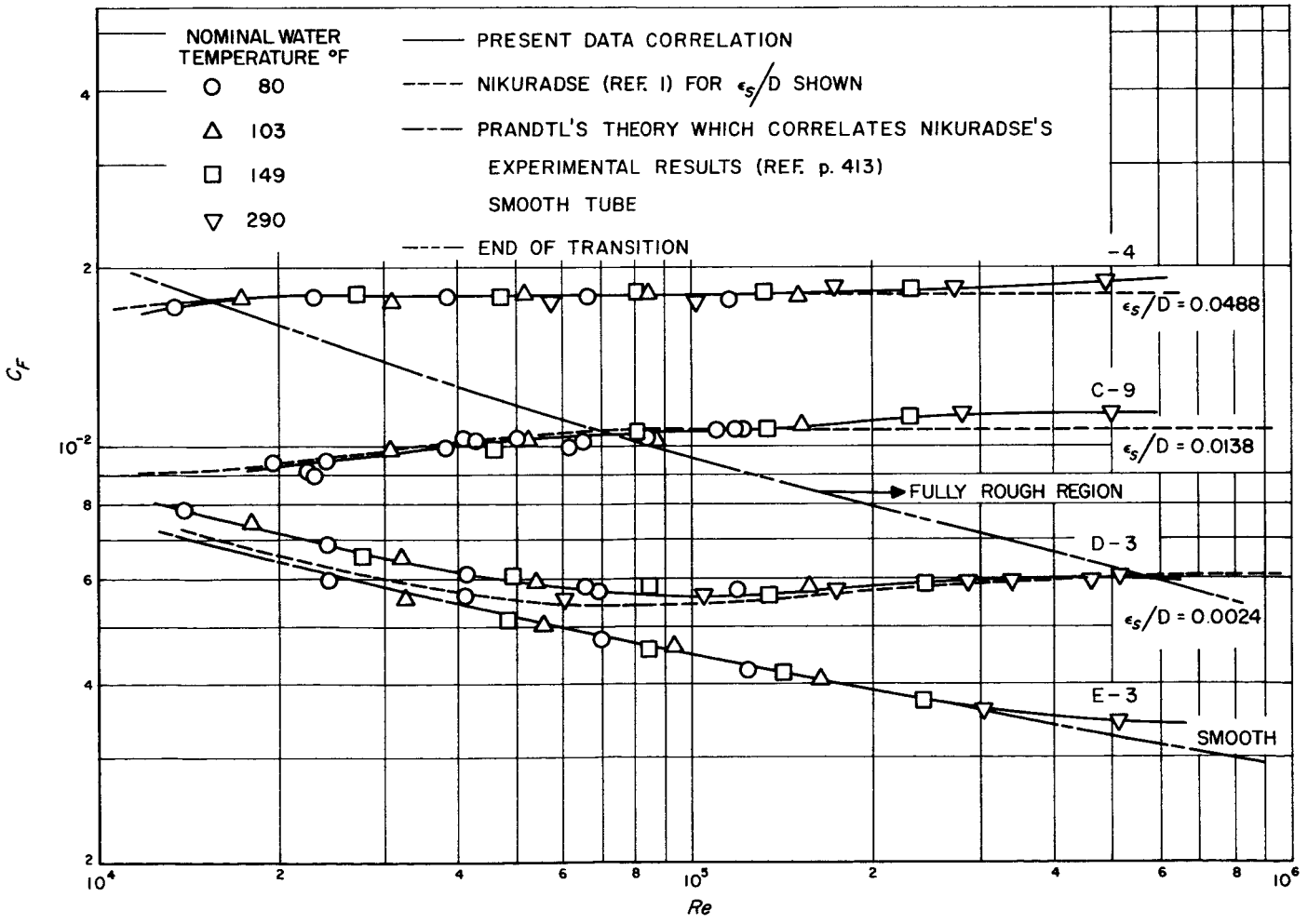

Fig. 4. Friction coefficient vs Reynolds number for tubes E-3, D-3, C-9, and A-4

by more than ±2.5% from a median curve anywhere within the Reynolds number range covered by the present results. Next, the effect of Pr was studied by examining Fig. 5 in which the ratio $2\,C_H/C_F$ is shown as a function of Pr for a fixed $Re = 1.5 \times 10^5$. Extremely close agreement is again observed between the results of Eagle and Ferguson and the present data within the range covered by both experiments, which extends from $Pr = 3$ to $Pr = 6$. Allen's data (Ref. 5) are represented by a single point on this graph, as his work was limited to one Prandtl number, and the same comments as before apply to the close agreement with these data.

Further inspection of Fig. 5 shows that the extrapolation of the present data to Prandtl numbers below 1.2, with the aid of Nunner's experimental point at Pr 0.72 (Ref. 3), yields a curve which gives a value of unity for $2\,C_H/C_F$ at a $Pr = 1$, a result which has been predicted by several theoretical approaches. The success of the theoretical prediction is due in part to a cancellation of errors introduced by the assumptions (cf. Ref. 4, p. 28).

In addition to the experimentally obtained results, a curve derived analytically by Rannie (Ref. 7) has also been entered in Fig. 5, and it is seen to fit the experimental results almost perfectly. On the other hand, it can be seen that the commonly used extrapolation for the ratio $2\,C_H/C_F$ to higher Prandtl numbers by means of the relation

$$\frac{2C_H}{C_F} = Pr^{-2/3}$$

underestimates this ratio, giving for example a value 25% below the measured one at a Pr of 6.

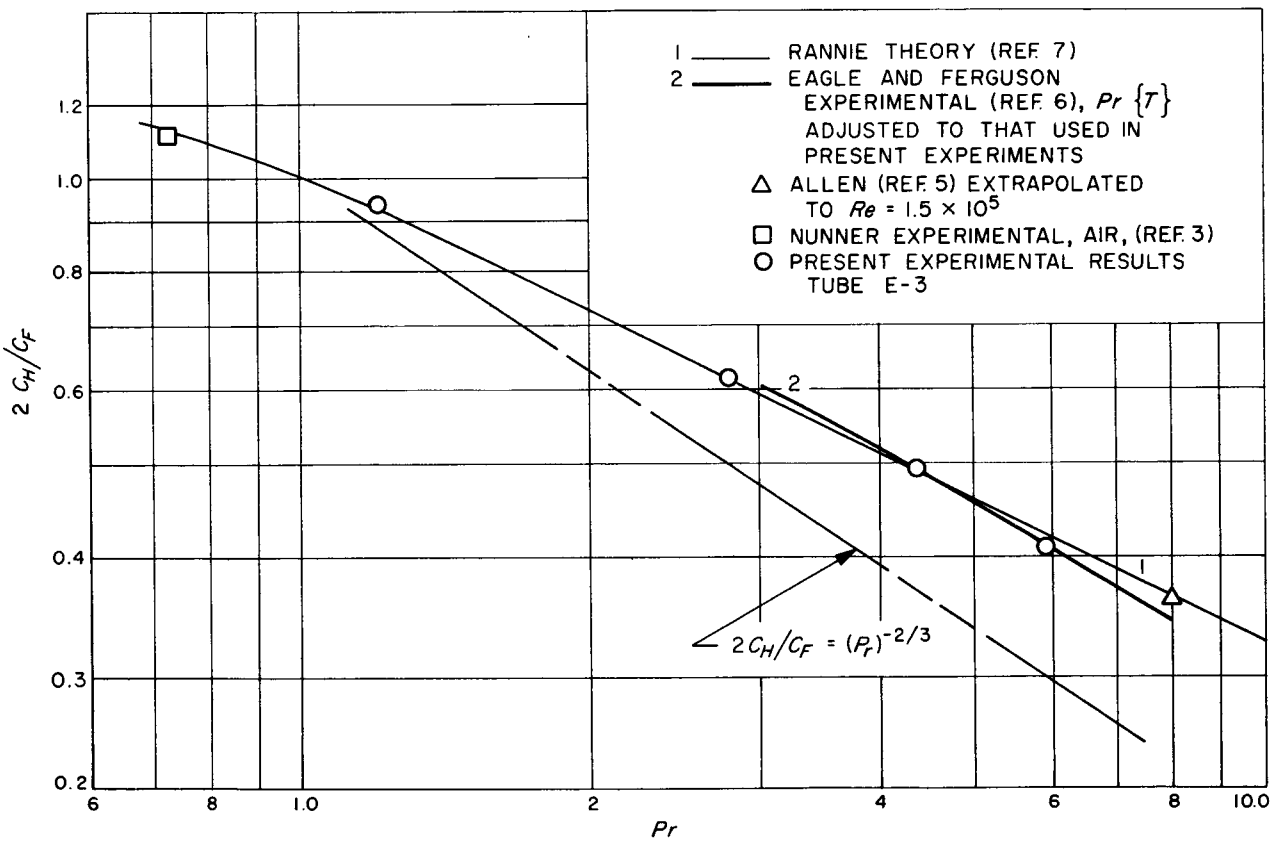

Fig. 5. Comparisons—Prandtl number influence on heat-transfer coefficients in smooth tubes at $Re = 1.5 \times 10^5$

IV. RESULTS FOR THE ROUGH TUBES

It is felt that the close agreement of the present results for the smooth tube with the most reliable published results lends confidence to the reliability of the experimental methods and therefore also to the results obtained with the rough tubes.

Three rough tubes were tested. The friction factor for all of these tubes is shown in Fig. 4. The pipe roughness was characterized by the length ε_s which is the hydraulic equivalent sand grain size. This size was determined by comparing, for the "hydraulically fully rough region," the friction factor of the present pipes with the formulation obtained by Nikuradse. It is noted that microscopic examination of the tube surfaces showed the character of the surfaces to be qualitatively similar to those produced by sand grains. Proceeding in the above manner, the effective roughness ratios were determined to be $\varepsilon_s/D = 0.0488$, 0.0138, and 0.0024, respectively. The shape of the curves of C_F vs Re is typical of those for sand-grain-type roughness in that they reach a minimum at an intermediate Re value and then gradually rise to a value beyond which the friction factor becomes insensitive to Reynolds number. This behavior differs from that for a naturally rough tube in which the friction coefficient continuously decreases in approaching the final asymptotic value at high Re values. For the tubes of the present experiments, the region from the point where the curve deviates from the behavior of a smooth tube up to the point at which the friction coefficient becomes essentially independent of Re is called the "transition region." The region beyond this point is termed the "fully rough region."

The heat transfer coefficients for the three rough tubes are shown in Figs. 6, 7, and 8, respectively, in which C_H is plotted as a function of Re for several Prandtl numbers. A similar plot for the smooth tube is shown in Fig. 9 for comparison. First it may be seen that, at any given Re and Pr, C_H increases with progressively higher roughness values, and correspondingly with higher friction coefficients. Examining next the shape of the curves at a given Pr, one notes the general tendency that C_H increases with Re in the transition region, which is the region in which the friction coefficient changes its behavior from that corresponding to a smooth tube to that of a fully rough tube. A maximum is reached in this region near the start of the fully rough behavior. In the hydraulically fully rough region, the heat transfer coefficient, unlike

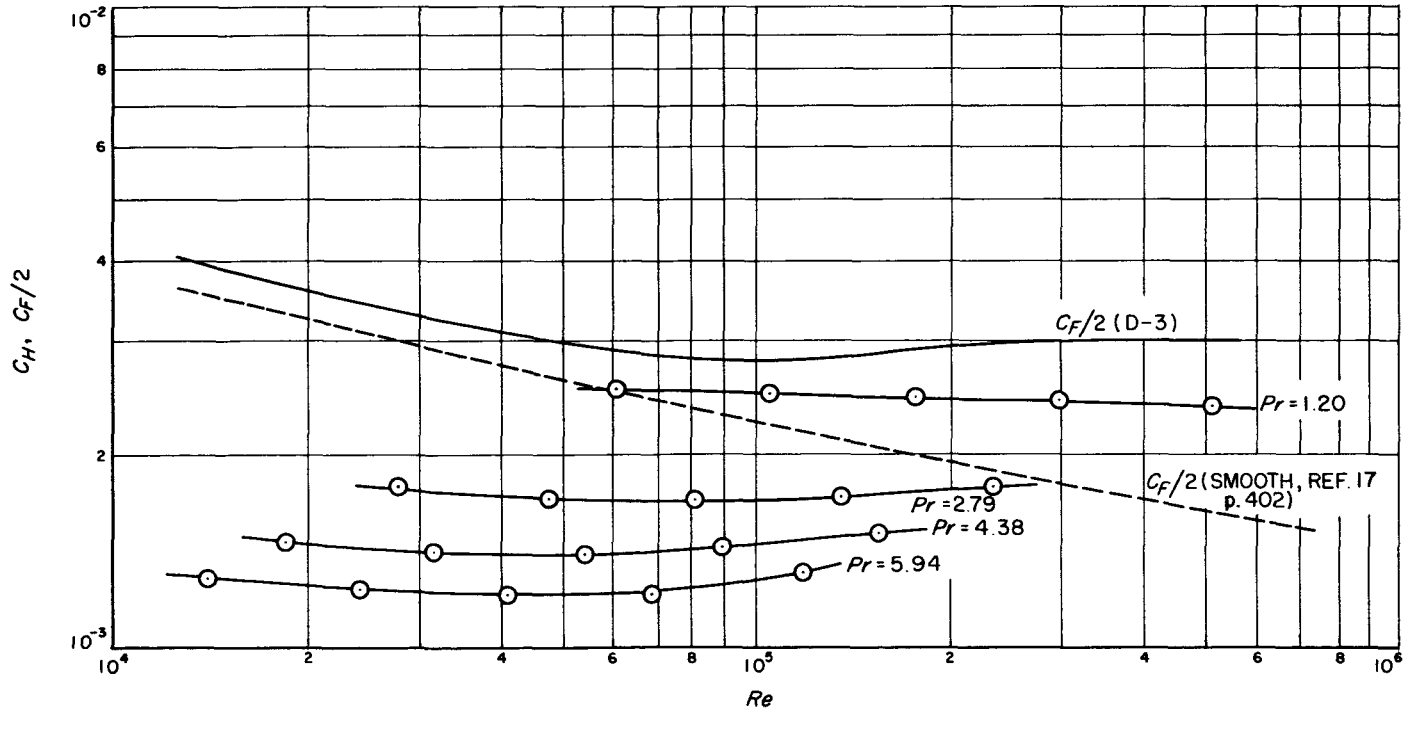

Fig. 6. Heat-transfer coefficient vs Reynolds number for tube D-3 ($\varepsilon_s/D = 0.0024$) at Prandtl numbers 1.20, 2.79, 4.38, and 5.94

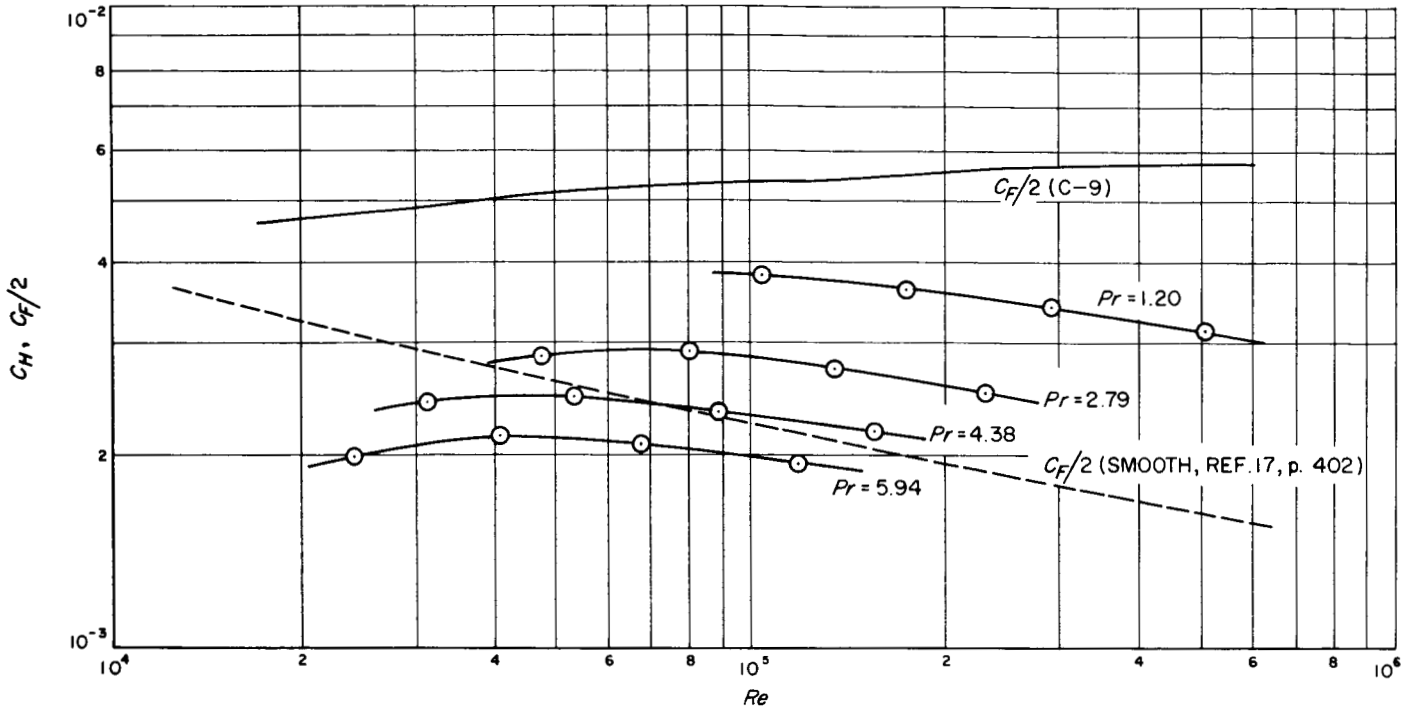

Fig. 7. Heat-transfer coefficient vs Reynolds number for tube C-9 ($\varepsilon_s/D = 0.0138$) at Prandtl numbers 1.20, 2.79, 4.38, and 5.94

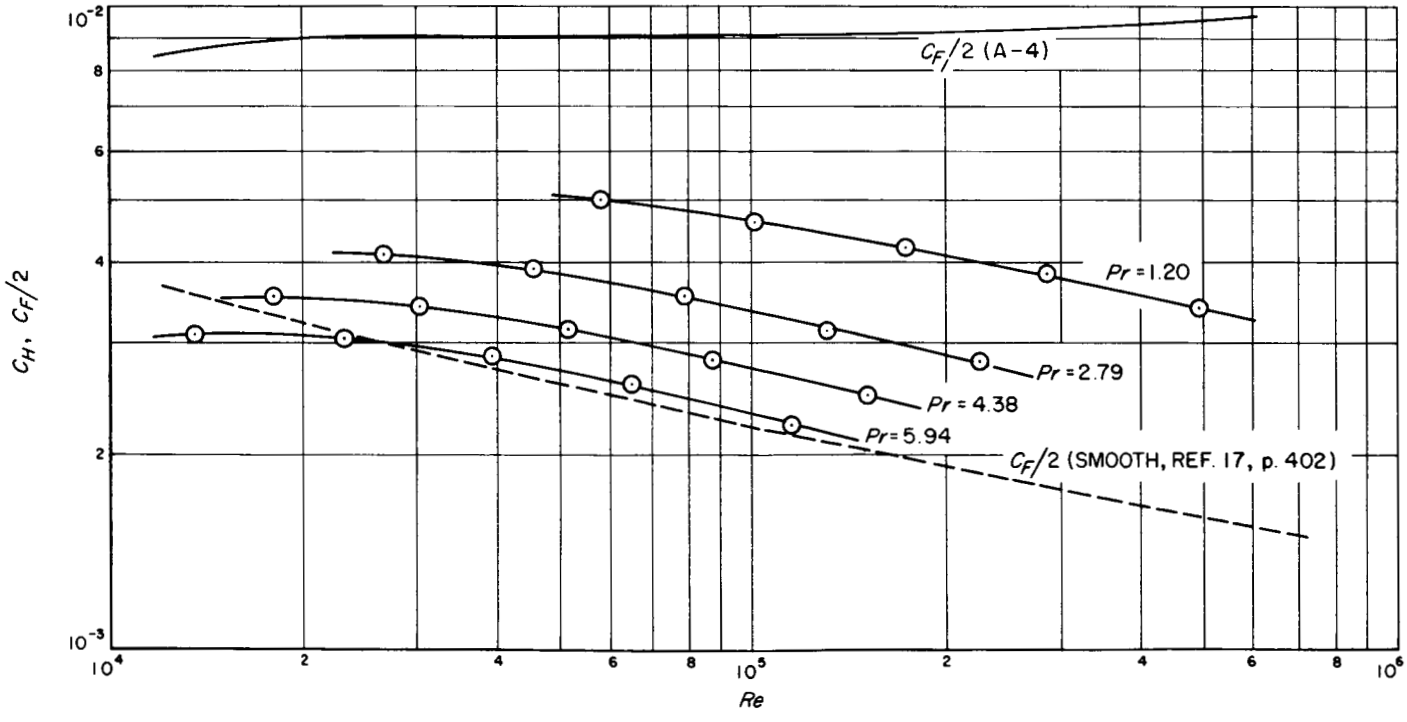

Fig. 8. Heat-transfer coefficient vs Reynolds number for tube A-4 ($\varepsilon_s/D = 0.0488$) at Prandtl numbers 1.20, 2.79, 4.38, and 5.94

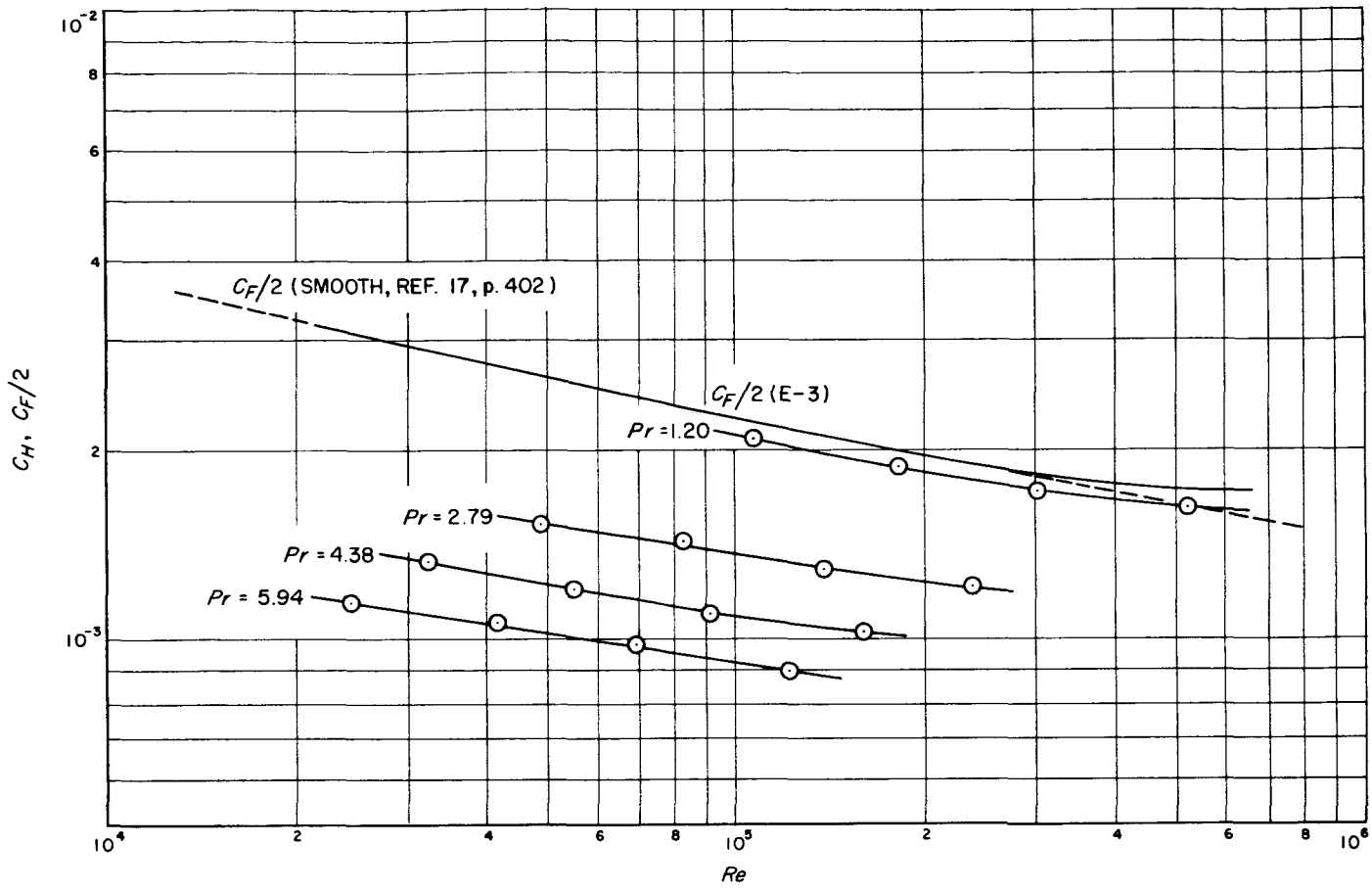

Fig. 9. Heat-transfer coefficient vs Reynolds number for tube E-3 (smooth) at Prandtl numbers 1.20, 2.79, 4.38, and 5.94

the friction coefficient, decreases monotonically. For the higher Prandtl numbers, the maximum of the curve is more pronounced. These tendencies are illustrated best for the tube with a roughness ratio of $\varepsilon_s/D = 0.0138$. For the Reynolds number range investigated in these experiments, the roughest tube ($\varepsilon_s/D = 0.0488$) covers mainly the C_H behavior at Re values beyond the maximum and the tube for the lowest roughness ($\varepsilon_s/D = 0.0024$) gives data principally in the range before this maximum.

Whether or not rough pipes are advantageous for engineering use depends on the specific application. In general, however, the ratio $2C_H/C_F$ is important along with C_H in considering the relative merit of heat transfer surfaces, the ratio being related to the heat transfer obtainable per unit of pumping power. Two graphs (Figs. 10 and 11) are shown in which this ratio ($2C_H/C_F$) is plotted as a function of Re for the different tubes. The first graph (Fig. 10) has been prepared for a Pr of 1.20 and the second (Fig. 11) for a Pr of 5.94. An inspection of Fig. 10 shows that, for the conditions of these tests, no gain is obtainable by roughening at the low Prandtl number. At the higher Pr of 5.94, however, it is apparent that there is at least one tube roughness value at each Re which gives a ratio $2C_H/C_F$ exceeding that of the smooth tube. It is interesting to note that this favorable ratio of C_H/C_F occurs in the transition region rather than in the fully rough region. More generally, the complete results of these experiments show that at low Prandtl numbers ($Pr < 3$) the $2C_H/C_F$ values can only be lowered by roughening; whereas for $Pr > 3$ it will always be possible to select a finite roughness so as to obtain $2C_H/C_F$ values somewhat above those for the smooth tube.

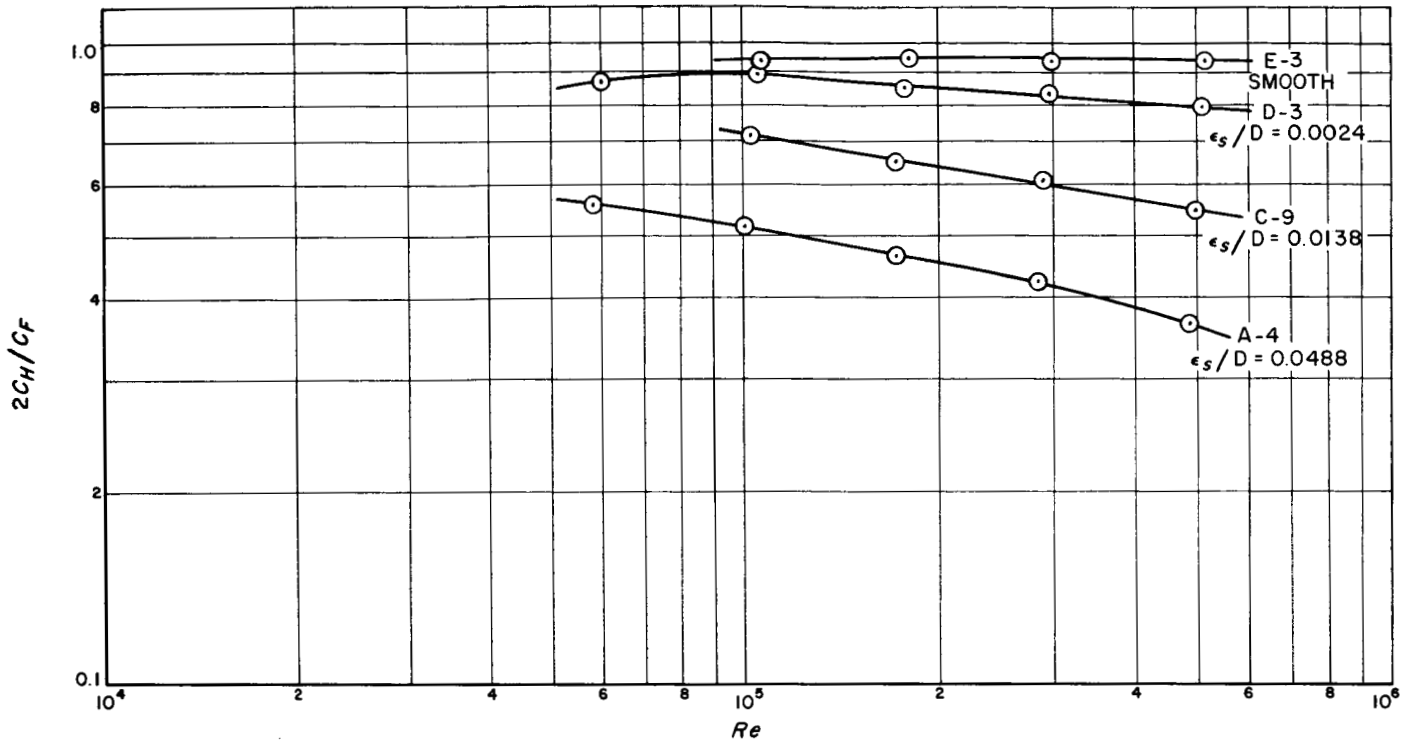

Fig. 10. Comparisons of heat-transfer and friction coefficients vs Reynolds number for $Pr = 1.20$

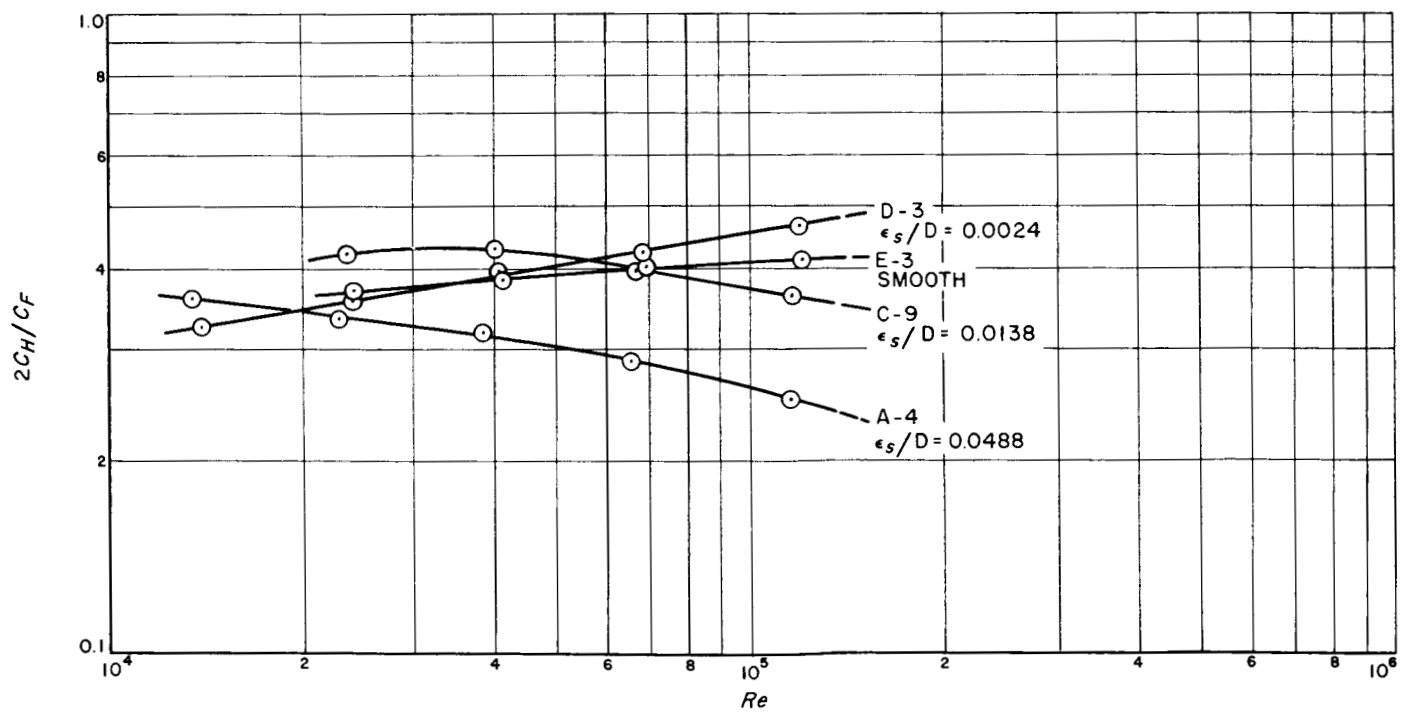

Fig. 11. Comparisons of heat-transfer and friction coefficients vs Reynolds number for $Pr = 5.94$

V. DERIVATION OF THE HEAT TRANSFER SIMILARITY LAW

Having presented the experimental data, let us now turn to some general analytical considerations regarding the heat transfer in rough tubes. Theoretical approaches to the problem of momentum transfer in smooth and rough tubes, as well as to the problem of heat transfer in a smooth tube, have been available for some time. These approaches have been based on similarity considerations and on the analogy between the turbulent diffusivities of heat and momentum. Because of the complex nature of turbulent flow, the theoretical work still must rely extensively on empirical information. However, the results of similarity theories permit the presentation of experimental results in their most general form by establishing the basic forms of the relationships between the essential parameters, in addition to specifying the significant parameters themselves.

As a direct consequence of widely applicable similarity assumptions, the "friction similarity law" can be developed (Ref. 4) for pipes having geometrically similar roughness, i.e., roughness that can be represented by a single length parameter. The basic similarity assumptions (cf., e.g., Ref. 8) are the "principle of Reynolds number similarity" and the "law of the wall similarity." For turbulent pipe flow, the first of these implies the existence of a region, away from the immediate vicinity of the wall, where the direct effect of viscosity on the mean flow is negligible. The second postulates the existence of a region close to the wall where the velocity distribution depends exclusively on the local conditions, y, τ_0, ρ, ν, and ε. The resulting friction similarity law may be written

$$\left(\frac{2}{C_F}\right)^{1/2} = -B \ln \frac{2\varepsilon}{D} + A\{\varepsilon^*\} - E \tag{3}$$

where ε is a representative length, say the roughness height. This is essentially the equation previously developed by Nikuradse starting from a somewhat different approach (Ref. 1). The symbol $\varepsilon^* \equiv \varepsilon u_\tau/\nu$ can be identified as $[Re\,(C_F/2)^{1/2}\,\varepsilon/D]$ as follows from the definitions of the respective terms, and $A\{\varepsilon^*\}$ is a general function determined empirically for each roughness shape. The function $A\{\varepsilon^*\}$ is expected to be different for different geometrical configurations. The constants B and E are universally valid for all roughness shapes, having been evaluated by Nikuradse as 2.50 and 3.75, respectively. The velocity distribution corresponding to Eq. (3) is given by

$$\frac{u}{u_\tau} = B \ln\left(\frac{y}{\varepsilon}\right) + A\{\varepsilon^*\} \tag{4}$$

Equation (4) is valid in a region close enough to the wall so that the shear stress can be considered constant ($y/R << 1$) and far enough from the wall so that Reynolds number similarity holds true.

The function $A\{\varepsilon^*\}$ for Nikuradse's sand-grain roughness is reproduced in Fig. 12. Equation (3) also illustrates how, by virtue of the analysis, it has become possible to reduce the experimental work in determining C_F. Instead of having to determine C_F as a function of the two parameters, Re and ε/D, it is now only necessary to determine the function $A\{\varepsilon^*\}$ which depends on the single parameter ε^*.

Following steps similar in nature to those which lead to the "friction similarity law" and including the above mentioned analogy between the turbulent diffusivities of heat and momentum, we shall now attempt to develop a general "heat transfer similarity law." This law should be applicable to rough as well as smooth tubes. The considerations will be subject to the restrictions listed below.

1. Fully turbulent (Re greater than about 2000), steady, pipe flow.
2. Hydrodynamically fully established flow in which the mean fluid motions are invariant with axial station.
3. Thermally fully established conditions whereby the radial temperature profile, referenced to the local wall temperature, is independent of axial location.
4. Constant fluid properties, i.e., constant density (ρ), viscosity (μ), thermal conductivity (k), and specific heat (c_p).
5. Surface roughness patterns which are statistically independent of circumferential or axial position provided that statistical samples are taken for regions much greater than the scale of the roughness elements.
6. Roughness patterns which are statistically geometrically similar from tube to tube with only a geometrical scale factor being different.

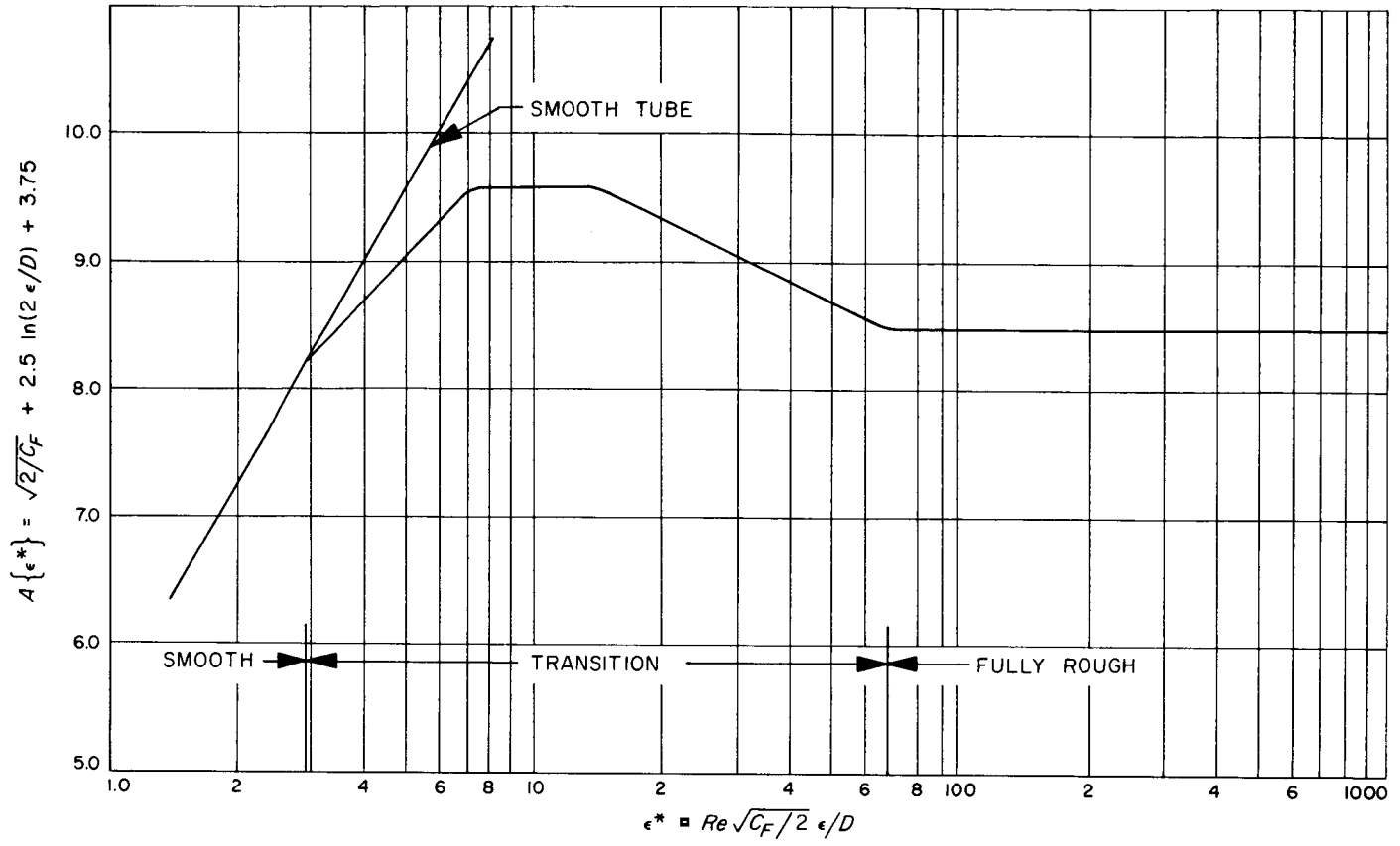

Fig. 12. Friction similarity function for close-packed sand-grain roughness

The velocities and temperatures being discussed are averaged both temporally and spatially in the circumferential and axial directions, and the spatial averaging is carried over distances greater than the size of the roughness elements.

The usual assumptions for the constant heat flux boundary condition then lead to the equations (cf., e.g., Appendix A of Ref. 7),

$$\left(\frac{\tau_0}{\rho}\right)\left(1+\frac{2y}{D}\right) = (\varepsilon_m + \nu)\frac{du}{dy} \tag{5}$$

and

$$-\left(\frac{q_0}{\rho c_p}\right)\left(1+\frac{2y}{D}\right) = \left(\varepsilon_h + \frac{\nu}{Pr}\right)\frac{dT}{dy} \tag{6}$$

for momentum (Eq. 5) and heat transfer (Eq. 6). The terms ε_m and ε_h are, respectively, the turbulent diffusivities for momentum and heat, defined from the temporal and spatial averages of the velocity-velocity and temperature-velocity products of the turbulent fluctuations.

Three essential further assumptions are then adopted: (1) The "law of the wall" used for the velocity and friction similarity laws is assumed to hold in the region of $2y/D << 1$. This law, which states that in the neighborhood of the wall $u = u\{y, \tau_0, \rho, \nu, \varepsilon\}$ also leads to the conclusion that

$$\frac{\varepsilon_m}{\nu} = f_1\{y^*, \varepsilon^*\} \tag{7}$$

(2) The Reynolds analogy, stating that

$$\varepsilon_h = \varepsilon_m \tag{8}$$

for the fully turbulent region of the flow, is assumed to be valid. And (3) the respective distance from the wall at which the velocity equals u_m and at which the temperature equals T_L are assumed to be the same.

The first of these assumptions has been verified as previously indicated. The latter two assumptions are the same as those used in smooth pipe theories by von Kármán (Ref. 9) and by Rannie (Ref. 7). The success of these smooth pipe theories is due in part to a cancellation of the errors introduced by these two assumptions. It is implied here that this same cancellation will occur for rough surfaces; this implication is supported by an analysis in Ref. 4 given for the case of the "fully rough" flow condition.

The heat transfer similarity law for geometrically similar rough surfaces is then a necessary consequence of the assumptions. The region between the rough wall and the distance y_m, where u_m and T_L occur, is resolved into two regions at the distance y_2 which is arbitrarily selected to be far enough from the wall that viscous shear stresses are negligible. The defining equation for C_H can then be written

$$\frac{1}{C_H} = \frac{\rho c_p u_m}{q_0}(T_w - T_2) + \frac{\rho c_p u_m}{q_0}(T_2 - T_L) \tag{9}$$

In the region between y_2 and y_m, a combination of the integrals of Eq. (5) and (6) yields

$$\frac{\rho c_p u_m}{q_0}(T_2 - T_L) = \frac{2}{C_F} - \frac{\dfrac{u_2}{u_\tau}}{\left(\dfrac{C_F}{2}\right)^{1/2}} \tag{10}$$

where use has been made of assumptions (2) and (3) and the identity $u_m/u_\tau \equiv (2/C_F)^{1/2}$. Using assumption (1), one can write

$$\frac{u_2}{u_\tau} = f_2\{y_2^*, \varepsilon^*\} \tag{11}$$

A dimensional analysis for the temperature difference $(T_w - T_2)$ based on the parameters of the law of the wall y_2, τ_0, ρ, ν, and ε and on the heat transfer parameters q_0, c_p, and k is then performed. The result can be written

$$\frac{\rho c_p u_m}{q_0}(T_w - T_2) = \frac{u_m}{u_\tau} f_3\{y_2^*, \varepsilon^*, Pr\} = \frac{1}{\left(\dfrac{C_F}{2}\right)^{1/2}} f_3\{y_2^*, \varepsilon^*, Pr\} \tag{12}$$

Then substituting Eq. (10), (11), and (12) into Eq. (9) and reorganizing the latter gives

$$\frac{\left(\dfrac{C_F}{2C_H}\right) - 1}{\left(\dfrac{C_F}{2}\right)^{1/2}} = f_3\{y_2^*, \varepsilon^*, Pr\} - f_2\{y_2^*, \varepsilon^*\} \tag{13}$$

Since y_2^* is an arbitrary constant number it can be dropped from the function and the resulting "heat transfer similarity law" is written

$$\frac{\left(\dfrac{C_F}{2C_H}\right) - 1}{\left(\dfrac{C_F}{2}\right)^{1/2}} + A = g\{\varepsilon^*, Pr\} \tag{14}$$

The constant, A, which is the $A\{\varepsilon^*\}$ value for the "fully rough" region, has been included to simplify the form of certain limiting cases of Eq. (14).

Examining Eq. (14) one sees that the experimental task of determining the heat transfer coefficient C_H is now reduced to that of obtaining the g-function which depends on the two variables ε^* and Pr; whereas without the foregoing analysis C_H had to be regarded as a function of the three parameters, ε/D, Pr, and Re. This simplification is analogous to the one which was made possible by the friction similarity law in connection with the determination of C_F. It should be reemphasized that in both cases the functions $A\{\varepsilon^*\}$ and $g\{\varepsilon^*, Pr\}$ are restricted to some specified type of geometrically similar roughness, and a new set of experiments is required for each roughness type.

It is of interest to point briefly to the limiting form of Eq. (14), as ε approaches 0 and the pipe approaches a smooth one. It is possible to show (Ref. 4) that for this limit

$$[g\{\varepsilon^*, Pr\} - A] \underset{\varepsilon \to 0}{\longrightarrow} F\{Pr\} \equiv \int_0^{y_2^*} \left[\frac{1}{\left(\dfrac{\varepsilon_m}{\nu}\right) - \dfrac{1}{Pr}} - \frac{1}{\left(\dfrac{\varepsilon_m}{\nu}\right) - 1} \right] dy^* \tag{15}$$

For sufficiently large values of y_2^*, as are being considered here, the integral of Eq. (15) becomes independent of the exact value of y_2^*. Substituting the limit of Eq. (15) into Eq. (14) gives the previously established heat transfer similarity law for smooth tubes. Rannie (Ref. 7) has evaluated $F\{Pr\}$ using a mathematical model for the relation $\varepsilon_m/\nu\{y^*\}$. Other evaluations of the function $F\{Pr\}$ have been made by several authors, in particular by von Kármán (Ref. 9) and more recently by Deissler (Ref. 10).

VI. EVALUATION OF THE HEAT TRANSFER SIMILARITY LAW

The results of the present experiments may be used to obtain a first check on the validity of the heat transfer similarity law as presented by Eq. (14). For evaluating ε^*, the equivalent sand-grain roughness ratio (ε_s/D) will be used. In terms of the friction similarity law this corresponds to selecting Nikuradse's value of $A = 8.48$ for the fully rough region. It may be pointed out that, having made this selection, the curve of $A\{\varepsilon^*\}$ vs ε^* is quite similar to that of Nikuradse for the entire range of ε^*, as is implied by the results shown in Fig. 4. Since Nikuradse's results have been shown to be consistent with the friction similarity law (Eq. 3), the use of ε_s/D assures compliance with that similarity law in the fully rough region prior to testing the heat transfer similarity law with the present results.

With this definition of roughness ratio, the results from the present experiments are plotted as "g" vs ε^* [$\varepsilon^* \equiv Re\,(C_F/2)^{1/2}\,\varepsilon_s/D$] in Fig. 13 for the four Prandtl numbers investigated. The fact that the curves, generated by the data points from three tubes of differing roughness, are nearly continuous is regarded as a significant substantiation of the heat transfer similarity rule (Eq. 14). At Prandtl number of 1.20, the match of the data from the different tubes is excellent; whereas at the highest Prandtl number there exists, in the region of overlap, some discrepancy between the data from the tubes with ratios $\varepsilon_s/D = 0.0488$ and $\varepsilon_s/D = 0.0138$. This discrepancy, which corresponds to approximately 8% in the heat transfer coefficient, could be ascribed to the basic inaccuracies of the experimental results and/or to the slight lack of geometrical similarity between the roughness *shapes* of these tubes.

The ε^* regions shown in Fig. 13 correspond to the respective regions in the $A\{\varepsilon^*\}$ curve for sand-grain roughness (Fig. 12). In the "smooth" region, the points from the tube with the lowest roughness ($\varepsilon_s/D = 0.0024$) approach, but remain slightly above, the horizontal broken lines representing the smooth tube experimental results. These smooth tube lines also correspond to the theoretical results of von Kármán and of Rannie in the form which is obtained by the substitution of Eq. (15) into Eq. (14). In the fully rough region ($\varepsilon^* > 67$), the curves become parallel on this log-log plot and tend toward a fixed positive slope.

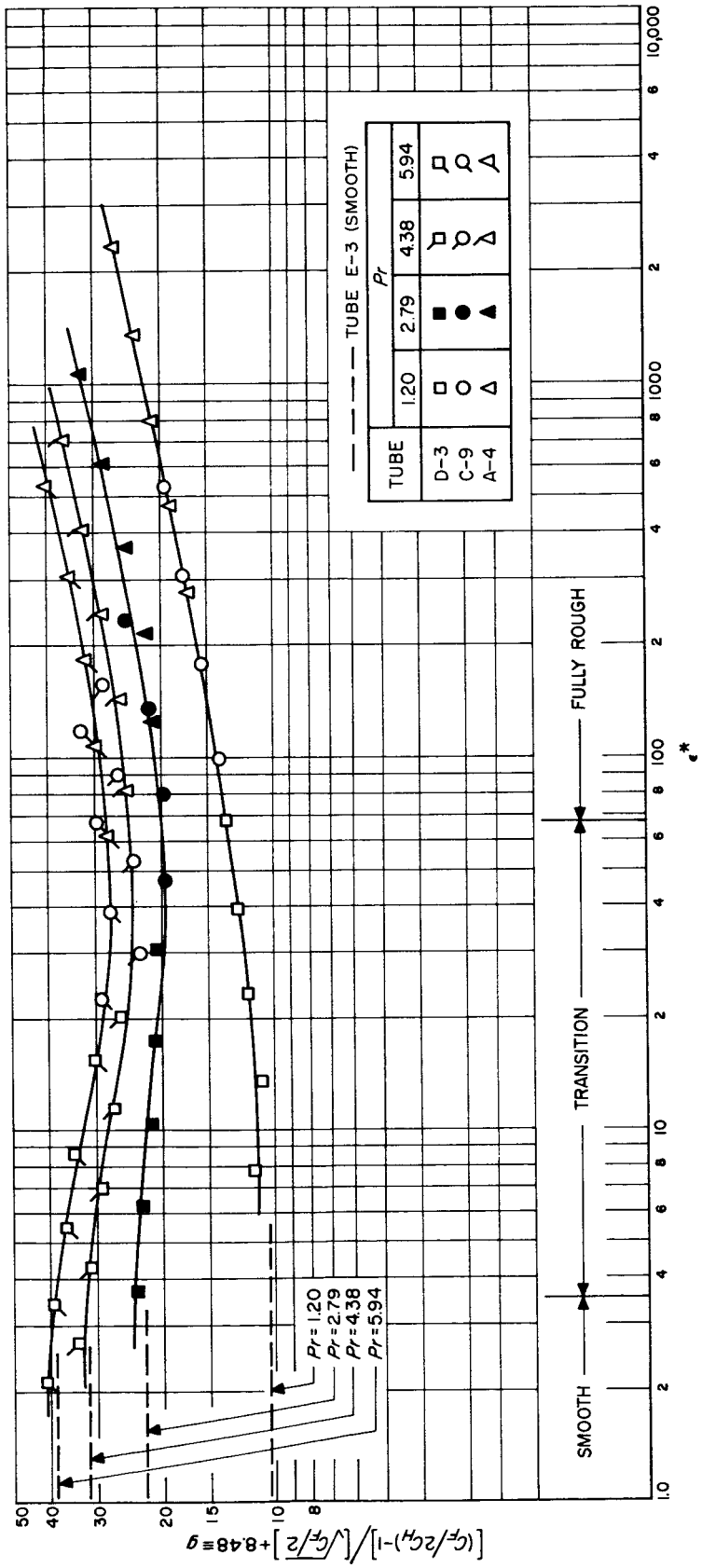

Fig. 13. Correlation of experimental results using the heat-transfer similarity law

VII. CAVITY VORTEX HYPOTHESIS[2]

The considerations leading to the derivation of the "heat transfer similarity law" were of a very general nature and did not require any detailed assumptions as to the type of flow which might take place near the rough surface. In this section we shall now introduce such an additional assumption by speculating that the rough wall can be imagined to consist of a series of small cavities and that the time-mean flow in and about these cavities consists of a pattern of one or more standing vortices. Such patterns have been observed in cavities of larger size in flow visualization experiments (Ref. 11). Such a flow pattern conforms to the cavity wall profile with a finite number of stagnation points between neighboring vortices. Thin boundary layers are formed on the cavity walls starting at alternate stagnation points and separating at the subsequent ones. The heat, once transmitted through the thin boundary layer, is assumed to be convected to the cavity opening with negligible temperature drop.

Further discussion is now limited to the region of "fully rough" hydraulic behavior. In this region the surface drag is independent of viscosity. This leads to the conclusion that the integrated axial component of the pressure forces on the roughness-cavity walls greatly exceeds the viscosity dependent shear stress acting on the same walls. The independence of the surface pressure drag from viscosity also implies that the time-mean flow pattern in each cavity is independent of viscosity. It follows from the above reasoning that the Reynolds number similarity assumption is still valid at the tips of the roughness elements, and it is thus permissible to set the distance y_2 (used in the development of Eq. 14) equal to ε, the roughness height, which is the same as the depth of the cavity. Following otherwise the same reasoning as before yields for Eq. (12)

$$\frac{\rho c_p u_m (T_w - T_g)}{q_0} = \frac{1}{\left(\frac{C_F}{2}\right)^{1/2}} f_3\{\varepsilon^*, \varepsilon^*, Pr\} \tag{16}$$

Recalling that $u_m/u_\tau \equiv (2/C_F)^{1/2}$, one may rearrange Eq. 16 into the form

$$C_{Hc} \equiv \frac{q_0}{\rho c_p u_g (T_w - T_g)} = \frac{1}{\frac{u_g}{u_\tau}\{\varepsilon^*\} f_3\{\varepsilon^*, Pr\}} \tag{17}$$

where u_g, T_g, and q_0 are, respectively, the spatial and temporal means of the velocity, the temperature, and the heat flux at the level of the tips of the roughness elements. The left-hand side of Eq. (17) is a Stanton number based on the temperature difference between the walls and the cavity opening and the velocity at the cavity opening. The quantity C_{Hc} is determined by the resistance to the heat flow through the cavity and it is called, therefore, the cavity heat transfer coefficient, or the cavity Stanton number.

Continuing the steps of the previous development, but letting $y_2 = \varepsilon$, brings Eq. (13) into the form

$$\frac{\left(\frac{C_F}{2C_H}\right) - 1}{\left(\frac{C_F}{2}\right)^{1/2}} = \frac{1}{\left(\frac{u_g}{u_\tau}\right)\{\varepsilon^*\} C_{Hc}\{\varepsilon^*, Pr\}} - \left(\frac{u_g}{u_\tau}\right)\{\varepsilon^*\} \tag{18}$$

For the fully rough conditions which are being considered, the function $A\{\varepsilon^*\}$ in the generalized velocity equation becomes a constant, A. Evaluating then the velocity at $y = \varepsilon$ from Eq. (4) shows that $u_g/u_\tau = A$, hence Eq. (18) reduces to

$$\frac{\left(\frac{C_F}{2C_H}\right) - 1}{\left(\frac{C_F}{2}\right)^{1/2}} = \frac{1}{AC_{Hc}\{\varepsilon^*, Pr\}} - A \tag{19}$$

and the g-function defined by Eq. (14) becomes

$$g_{FR} = \frac{1}{AC_{Hc}\{\varepsilon^*, Pr\}} \tag{20}$$

This equation lends a physical meaning to the function g in the fully rough region, showing that it is inversely proportional to the cavity Stanton number. The cavity Stanton number, in turn, depends only on Pr and ε^*, where ε^* may be regarded as the Reynolds number based on the characteristics of the cavity.

[2]For a more complete discussion of the cavity vortex hypothesis consult Appendix VII of Ref. 4.

Recalling that for the fully rough condition the mean flow patterns in the cavities must be independent of both the pipe Reynolds number and the roughness ratio, one may now go even further by attempting to compute the coefficient C_{Hc}. The general approach to this step will be briefly outlined. It will be assumed that the heat transfer coefficient, $C_{H_{vi}}$, for any of the several short boundary layers in the cavity can be approximated by a relation of the type

$$C_{H_{vi}} = K_{vi} (Re_{vi})^{-p} (Pr)^{-m} \tag{21}$$

where $C_{H_{vi}}$ is the average Stanton number based on the temperature and velocity locally external to the boundary layer and the local heat flux normal to the wall, and where Re_{vi} is the Reynolds number based on the same velocity and the length of the i^{th} boundary layer segment. By combining the effects of the several boundary layer segments as estimated by Eq. (21) and by using the previously stated assumptions of the cavity vortex hypothesis, the overall cavity Stanton number for fully rough flow is found to be

$$C_{Hc} = \frac{1}{Ak_f} (\varepsilon^*)^{-p} (Pr)^{-m} \tag{22}$$

or by Eq. (20)

$$g_{FR} = k_f (\varepsilon^*)^p (Pr)^m \tag{23}$$

where k_f is a constant dependent only on the particular type of roughness shape being considered. The constant exponents p and m on the other hand should be universally valid in accordance with the assumptions leading to Eq. (21).

The predictions embodied in Eq. (23) may now be compared with the results of the present experiments. An inspection of the data from the present experiments as presented in Fig. 14 shows that in the "fully rough" region the function g may be presented in the form proposed by Eq. (23), with $k_f = 5.19$, $p = 0.20$, and $m = 0.44$.

The fact that the experimental results can be cast into the form of Eq. (23) lends a modest degree of support to the concept of cavity-vortex flow. Some additional encouragement may be derived from the fact that the exponents p and m of the cavity Reynolds number and the Prandtl number, respectively, are of the same magnitude as the corresponding exponents which occur in equations of the form of Eq. (21) written for various boundary layer problems. A further check may be obtained by testing the prediction that other types of roughnesses should lead to a g-function which, in the fully rough regime, differs from the present one only in the magnitude of the constant k_f. As will be seen below, Nunner's data are in agreement with this prediction.

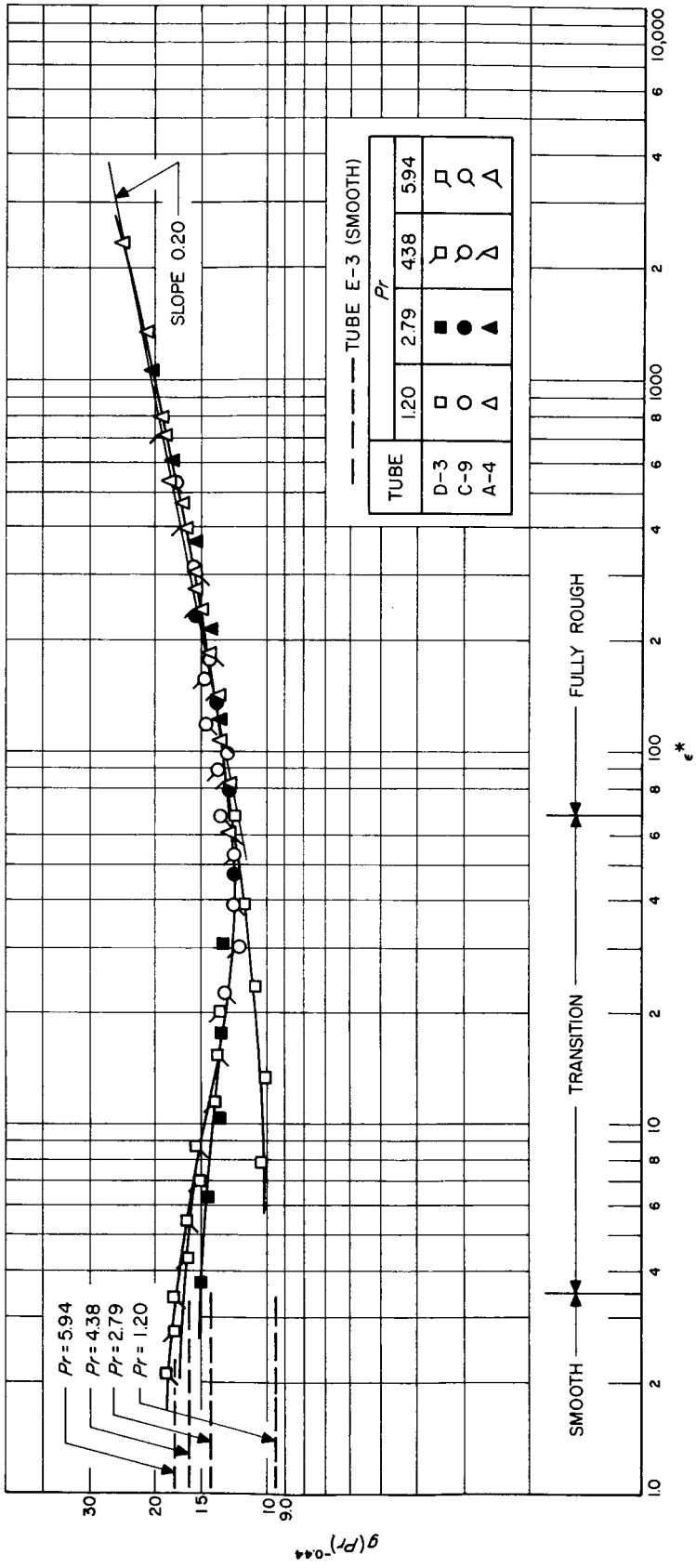

Fig. 14. Correlation of experimental results using the heat-transfer similarity law and a power law for Prandtl number

VIII. COMPARISON WITH PREVIOUS WORK

As mentioned previously, very extensive experiments were conducted by Nunner (Ref. 3) with air as a working fluid. The roughnesses in most of Nunner's work were produced by rings located at regular intervals in pipes. This roughness was, therefore, two-dimensional in nature. The effects of various sizes, cross-sectional shapes and spacings of such rings were investigated. The data from Nunner's tubes B-20 and D-20, which have differing roughness heights but have geometrically similar roughness shape, may be represented by a single g-function as is shown in Fig. 15. This fact may be taken as additional support for the heat transfer similarity law, Eq. (14). The curve generated by Nunner's data is seen to be parallel to that attained for the tubes with sand grain roughnesses of the present experiment. This fact is in agreement with the special predictions based on the model of the cavity vortex, as was just mentioned. It may further be noted that the points for different ring geometries (tubes D-5, D-2, and A-20) also fall on the curve formed by the data for the B-20 and D-20 tubes. This feature, which is most useful for engineering applications, is beyond what could have been predicted by any of the theoretical considerations given in this report. It should be emphasized, however, that, although differing roughness geometries of the same class (say all two-dimensional) may lead to the same single g-function, such a coincidence is not a general rule. As seen in Fig. 15, the three-dimensional sand grain roughnesses of the present experiments lead to a different g-curve than the roughnesses used by Nunner. As a consequence, rough pipes which show identical friction characteristics may lead to a different heat transfer performance, and one type of roughness may be preferable to another for this reason. The three-dimensional roughness of the present paper, for example, by virtue of the lower values for g, would show somewhat higher ratios of C_H/C_F than the two-dimensional roughness investigated by Nunner.

For completeness, additional experimental results have also been entered in Fig. 15, in particular those obtained with galvanized pipes and a "Karbate"[3] pipe by Smith and Epstein (Ref. 12) and those obtained with a cast iron pipe by Nunner (Ref. 3). These data fall mostly in a transition region where the friction factor changes with Reynolds number. It is seen that the results of the galvanized pipes may be adequately represented by a single curve on the g vs ε^* graph. From this, one may conclude that there exists a certain statistical similarity between the roughnesses of galvanized pipes of various sizes. The type of roughness represented by the "Karbate" and by the cast iron pipe, however, are probably geometrically dissimilar from that of the galvanized pipe. This is certainly plausible, but it means that all "natural" roughnesses may not be considered as a single class. It may also be noted that on the g vs ε^* graph the results of the cast iron pipe of Nunner's fall approximately on the extension of the straight line determined by his results for tubes with two dimensional roughnesses. As was just shown, however, one may not conclude from this coincidence that the curve for the two dimensional ring roughness is a universal one.

Various experimental data are compared further by means of Fig. 16. In this figure the quantity C_H/C_F divided by the corresponding ratio for a smooth tube (C_{HS}/C_{FS}) at the same Re and Pr is plotted as the ordinate, and the ratio C_F/C_{FS} is the abscissa. The symbol C_{FS} designates the friction factor of the smooth tube at the given Re. In general, high values of C_H/C_F at high values of C_H are desirable for heat exchanger designs. Thus the data represented by curve 1 would seem to be the most interesting of those presented. These data, taken from well known experiments by Fortescue and Hall (Ref. 13) were carried out in the course of the design of the cooling system for the Calder Hall reactor. The flow in this case took place in an annular passage. Heat was transferred from the inner surface only and this surface was provided with transverse fins extending partially across the flow passage. The fluid was a gas with a $Pr \simeq 0.7$. The results are particularly remarkable in that the points, corresponding to several different fin geometries, on curve 1 are well above unity. On the basis of concepts deriving from the Reynolds analogy (cf. Ref. 4, p. 160) a ratio of $(C_H/C_F)/(C_{HS}/C_{FS})$ greater than 1.0 should not be expected for a fluid with a Prandtl number close to 1.0. The flow in question, however, takes place in an annulus rather than in a pipe, and the adiabatic outer surface of the annulus was smooth. Estimating the friction coefficient based on the finned surface alone transposes the maximum point on curve 1 to the location (1′) as shown in Fig. 16. This new point is at approximately 0.9 which is no longer in disagreement with the predictions from Reynolds analogy. Nevertheless, even after this adjustment the surface investigated by Fortesque and Hall appears to have excellent characteristics for use in heat exchanger designs. It provides

[3]Trade name for a resin bonded graphite made by National Carbon Company.

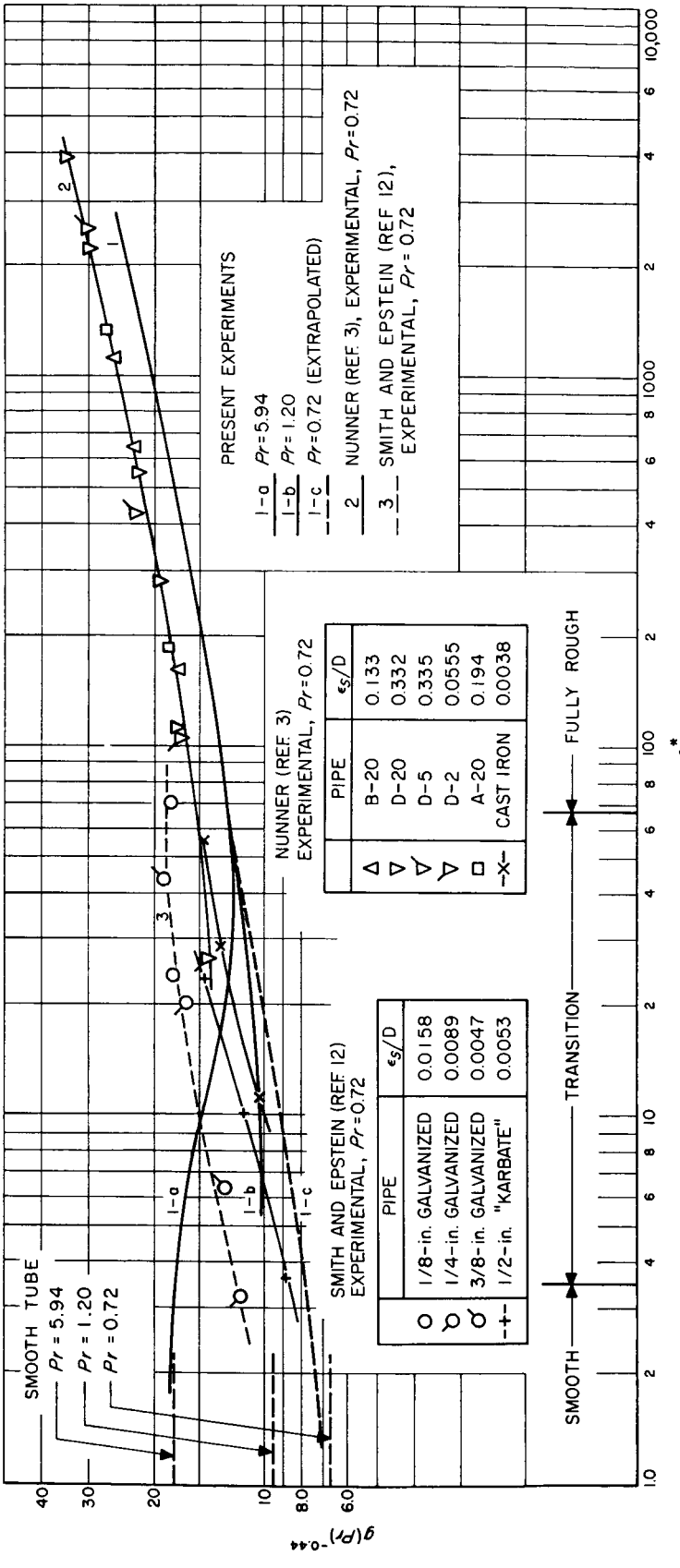

Fig. 15. Comparisons—rough tube heat-transfer experimental results and theories

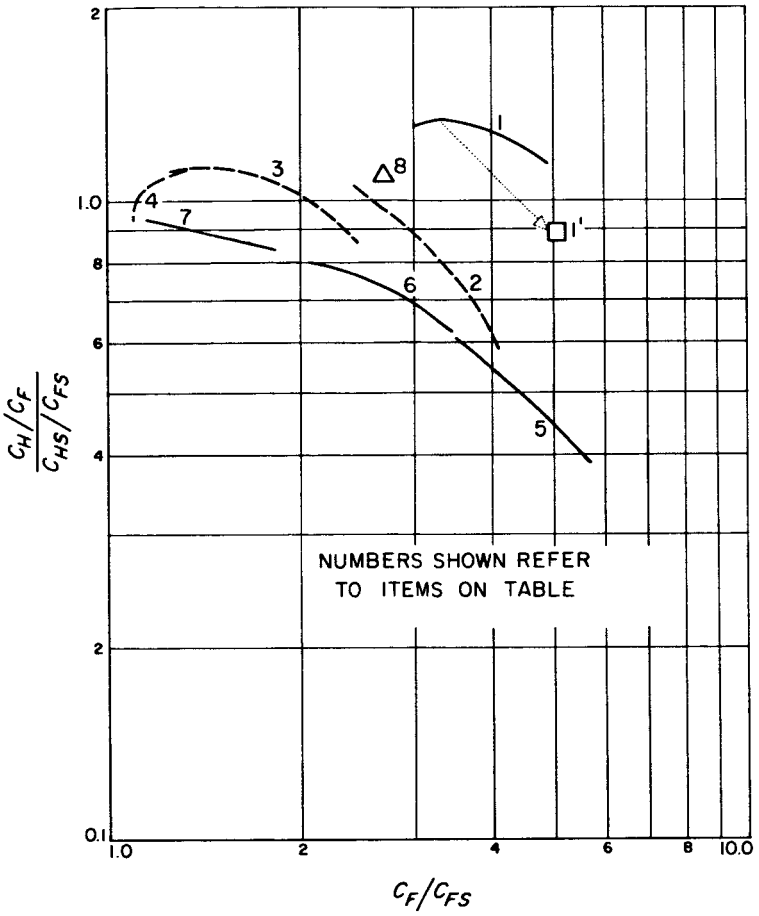

Item	Investigator	Roughness geometry	Reynolds number	Prandtl number	Remarks
1	Fortesque and Hall (Ref. 13)	Transverse fins on inner wall of an annulus, Fin root dia. $\cong$ 1.4 in. Channel dia. $\cong$ 4.0 in. Fin pitch = 3/16 in. Tip-to-root-dia. ratio of fins 1.3 to 1.9	Not given	~ 0.7	Combination of outer and inner wall effects in C_F terms
1′	Same	Same		~ 0.7	C_F terms computed on the basis of the inner, heat-transferring surface only
2	Present Investigation	Close-packed, granular roughness in pipe Tube A-4, ε_s/D = 0.049	$1.4 - 11.5 \times 10^4$	6.0	
3	Same	Tube C-9, ε_s/D = 0.014	$1.4 - 11.5 \times 10^4$	6.0	
4	Same	Tube D-3, ε_s/D = 0.0024	$1.4 - 11.5 \times 10^4$	6.0	
5	Same	Tube A-4, ε_s/D = 0.049	$5.8 - 51.0 \times 10^4$	1.2	
6	Same	Tube C-9, ε_s/D = 0.014	$5.8 - 51.0 \times 10^4$	1.2	
7	Same	Tube D-3, ε_s/D = 0.0024	$5.8 - 51.0 \times 10^4$	1.2	
8	Grass (Ref. 14)	Cross-grooved pipe Groove depth/Dia. = 0.005	3.7×10^4	~ 6.0 Assumed for water	

Fig. 16. Comparisons of experimental heat-transfer results for rough surfaces in relation to smooth surfaces

a heat transfer coefficient approximately 5 times that of a smooth tube with a decrease of only about 10% in the ratio of C_H/C_F over that of a smooth tube.

Next it may be noted that portions of curves 2, 3, and 4 also reach ordinates greater than unity. All of these curves were obtained from the present experiments for a $Pr = 6.0$. As discussed before in connection with Fig. 11, there are regions at high Pr in which a rough tube exceeds the ratio of C_H/C_F of a smooth tube. The flow in these instances takes place usually in the transition range between "smooth" and "fully rough" behavior. The top portions of the three curves mentioned correspond to this type of flow, and it is also believed that point 8 can be explained in this way. The data for this point were obtained by Grass (Ref. 14) with water ($Pr \simeq 6.0$ probably) in pipes with cross grooves.

Several analytical expressions for the heat transfer in rough tubes have also been developed previous to the present work. Of these, the ones by Nunner and by Martinelli are perhaps known best.

Nunner (Ref. 3) proposed a model in which the flow field was divided into two portions by an imaginary grid. As a first approximation he postulated this grid to exist at the outer edge of the laminar sublayer that would exist at the given Re if the tube were smooth. A form drag is produced at the grid which accounts for the observed increase in C_F of the rough tube over the smooth tube, and the grid benefits the heat transfer only insofar as the turbulent diffusivity in the central flow is increased by the grid's presence. With this model he developed the relation

$$C_H = \frac{\frac{C_F}{2}}{1 + 1.5\, Re^{-1/8}\, Pr^{-1/6}\left[\left(\frac{PrC_F}{C_{FS}}\right) - 1\right]} \tag{24}$$

A fair correlation of Nunner's experimental results at $Pr \simeq 0.7$ is obtained with this expression. In Fig. 17 a comparison of this, and other theoretical expressions, is made with the present experiments. For this, the ratio $2C_H/C_F$ is plotted vs Pr for $Re = 1.5 \times 10^5$ and $\varepsilon_s/D = 0.049$ or $C_{F_{FR}} = 0.018$. The latter conditions correspond to the data shown for the roughest tube of the present experiments. From the inspection of this figure one must conclude that Eq. (24) does not adequately predict the present results, particularly at high Prandtl number. Equation (24) also implies that there is a unique relationship between the friction factor and the heat transfer coefficient of a rough pipe, which relationship is independent of the type of roughness. The existence of such a relationship is not corroborated by the present experiments and analysis. One may further note that Eq. (24) cannot be arranged in a form such that

$$\frac{\left[\left(\frac{C_F}{2C_H}\right) - 1\right]}{\left(\frac{C_F}{2}\right)^{1/2}} = g\{\varepsilon^*, Pr\} - A \tag{25}$$

which is the universal form proposed previously. It was also noted in conjunction with the discussion of Fig. 15 that Nunner's *experimental* results as well as the present experimental results are in agreement with this universal form.

A second equation for the heat transfer which is frequently quoted is that developed by Martinelli (Ref. 15):

$$\frac{2C_H}{C_F} = \frac{1}{5\left(\frac{C_F}{2}\right)^{1/2}\left(Pr + \ln(1 + 5\,Pr) + \frac{1}{2}\ln\left[\left(\frac{C_F}{2}\right)^{1/2}\frac{Re}{60}\right]\right)} \tag{26}$$

This equation differs from that derived by Martinelli for smooth tubes only by the omission of the temperature ratio $(T_w - T_e)/(T_w - T_L)$ in the numerator. Martinelli suggested that the above equation might also apply to rough tubes, the effect of roughness entering the equation simply through the increase in C_F. The omission of the temperature ratio has relatively little effect as this term is usually just slightly less than 1.0 and rarely below 0.8. This equation is also compared to the present data in Fig. 17. Again the effect of Pr is not properly predicted and again a unique relationship between C_H and C_F is implied which is in contradiction to the findings of this paper. It may be pointed out, however, that Martinelli's equation can be written in the general form suggested (Eq. 25) with the g-function being

$$g\{\varepsilon^*, Pr\} = 5\left[(Pr - 1) + \ln(1 + 5\,Pr) + \frac{1}{2}\ln\varepsilon^*\right] + 8.71 - A\{\varepsilon^*\} \tag{27}$$

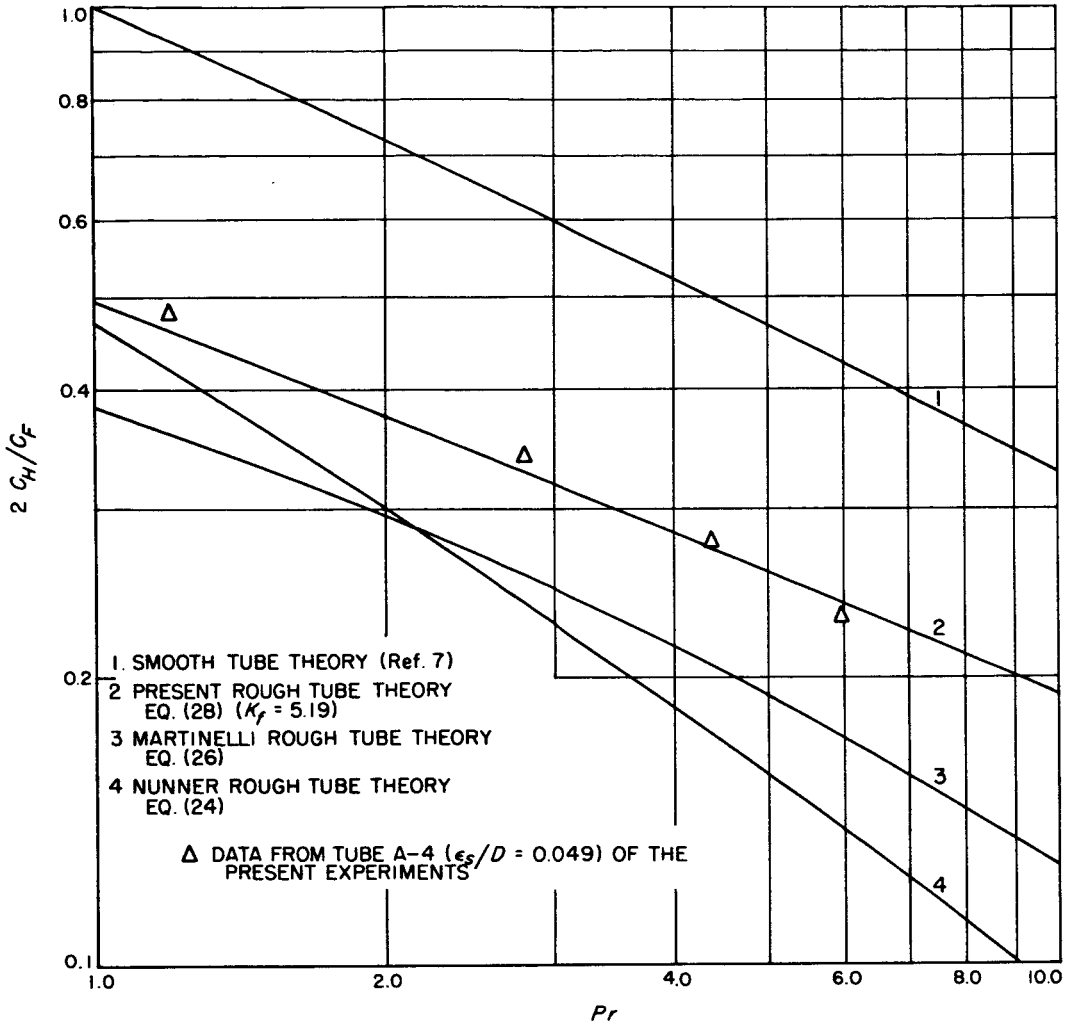

Fig. 17. Comparisons of rough tube theories at $Re = 1.5 \times 10^5$ and $\epsilon_s/D = 0.049$ ($C_{FFR} = 0.018$)

IX. APPLICATION OF THE DATA

For designing a heat exchanger, a knowledge of the coefficients $C_H\{Re, \varepsilon/D, Pr\}$ and $C_F\{Re, \varepsilon/D\}$ is a prerequisite. It will be indicated, on the basis of the generalized results, how it is possible to obtain rather complete information on these coefficients for a minimum of experimental results obtained with geometrically similar roughnesses. In the example to be discussed, we consider the type of roughness which was used for the present experiments, that is, a close-packed granular type. The size of the roughness, as discussed before, was established as a hydraulic equivalent by comparison with Nikuradse's sand-grain roughness results in the fully rough region. It is reasonable, as was indicated in the discussion of Fig. 4, to assume that the friction characteristics in the other flow regions are properly represented by Nikuradse's function $A\{\varepsilon^*\}$ which is shown in Fig. 12.

If now the universal presentation of the heat transfer results in terms of the g-function (cf. Fig. 14) is accepted as valid for the present roughness, the derived coefficients C_H and C_F can be computed for a wide range of the variables Re, ε_s/D, and Pr. The introduction of the g-function and the parameter ε^* thus allows an extension of the data beyond the range of Re and ε_s/D actually covered by the tests, without exceeding the experimental range of ε^*. It also allows more exact interpolations between the data points.

To show explicitly the results of the preceding derivation, the curves of $C_H\{Re, \varepsilon_s/D\}$ and $2C_H/C_F\{Re, \varepsilon_s/D\}$ shown in Fig. 18 and 19 are presented. These were generated by means of Fig. 12 and 14 and Eq. (3) and (14) with the universal constants B and E being taken as 2.5 and 3.75, respectively. Corresponding to the use of the sand-grain equivalent roughness ratio, the value of A was set at 8.48. Figures 18 and 19 apply for Prandtl number of 6.0. Clearly, similar charts could be generated for any Prandtl number in the range of the experiments, 1.2 to 6.0, and furthermore, slight extrapolations to say $Pr = 0.7$ and $Pr = 10$ may also be permissible. The necessary extrapolation of the function $g(Pr)^{-0.44}\{\varepsilon^*; Pr\}$ to $Pr = 0.7$ between the "smooth" and "fully rough" limits is shown as line 1-c in Fig. 15. The authors are preparing design charts similar to Fig. 18 and 19 for differing Prandtl numbers. These will be published at some future time.

For the case of "fully rough" conditions the information in Fig. 18 and 19 can be expressed in closed analytical form based on the cavity vortex hypothesis. Thus

$$C_{H_{FR}} = \frac{\frac{C_{F_{FR}}}{2}}{1 + \left(\frac{C_{F_{FR}}}{2}\right)^{1/2}\left(k_f\left[Re\left(\frac{C_{F_{FR}}}{2}\right)^{1/2}\frac{\varepsilon_s}{D}\right]^{0.2}(Pr)^{0.44} - 8.48\right)} \tag{28}$$

where

$$\frac{\varepsilon_s}{D} = \exp\left\{\frac{3.0 - \left(\frac{C_{F_{FR}}}{2}\right)^{-1/2}}{2.5}\right\} \tag{29}$$

Equation (29) is an inversion of Eq. (3). The constant k_f depends on the roughness form. For the granular close-packed roughness of the present experiments, $k_f = 5.19$. For the variety of two-dimensional roughnesses investigated by Nunner, $k_f = 6.37$. In the latter case experimental verification is limited to $Pr = 0.7$. Thus, using Eq. (28) and (29), one may compute the heat transfer coefficient given either the roughness ratio or the friction coefficient.

From an inspection of the figures presented, several features of interest in heat exchanger design may be noted:

1. For a wide range of Reynolds number and Prandtl number an improvement by a factor of two to three in the Stanton number can be obtained by substituting rough tubes for smooth tubes. With the present type of tubes, however, no higher factors should be expected.

2. There is a limit for any combination of Reynolds number and Prandtl number beyond which increases in roughness, while increasing C_F, will no longer increase C_H.

3. For any given roughness ratio and Prandtl number, the $C_H\{Re\}$ curves and the $C_H/C_F\{Re\}$ curves both have maxima. These occur in or near the transition region for the respective roughness ratios.

4. At the higher Prandtl numbers large improvements in Stanton number due to roughening can be achieved with little or no loss in C_H/C_F; in fact, at $Pr = 5.94$, roughness ratios can be selected that will increase C_H/C_F values by as much as 10% over those of the smooth tube.

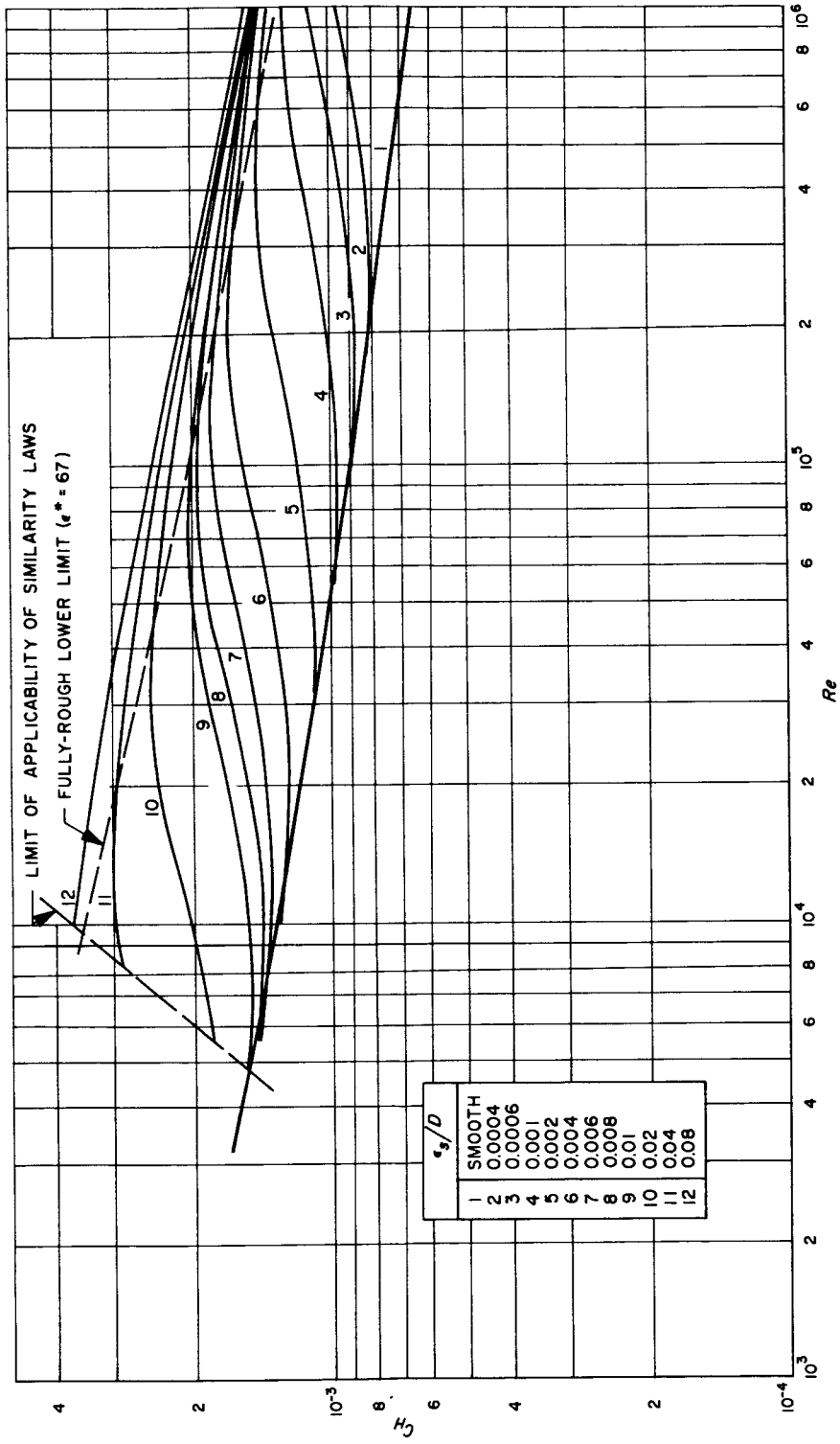

Fig. 18. Heat-transfer coefficient vs Reynolds number for $Pr = 6.0$, generated from the similarity functions $g\{\epsilon^*; Pr\}$ and $A\{\epsilon^*\}$

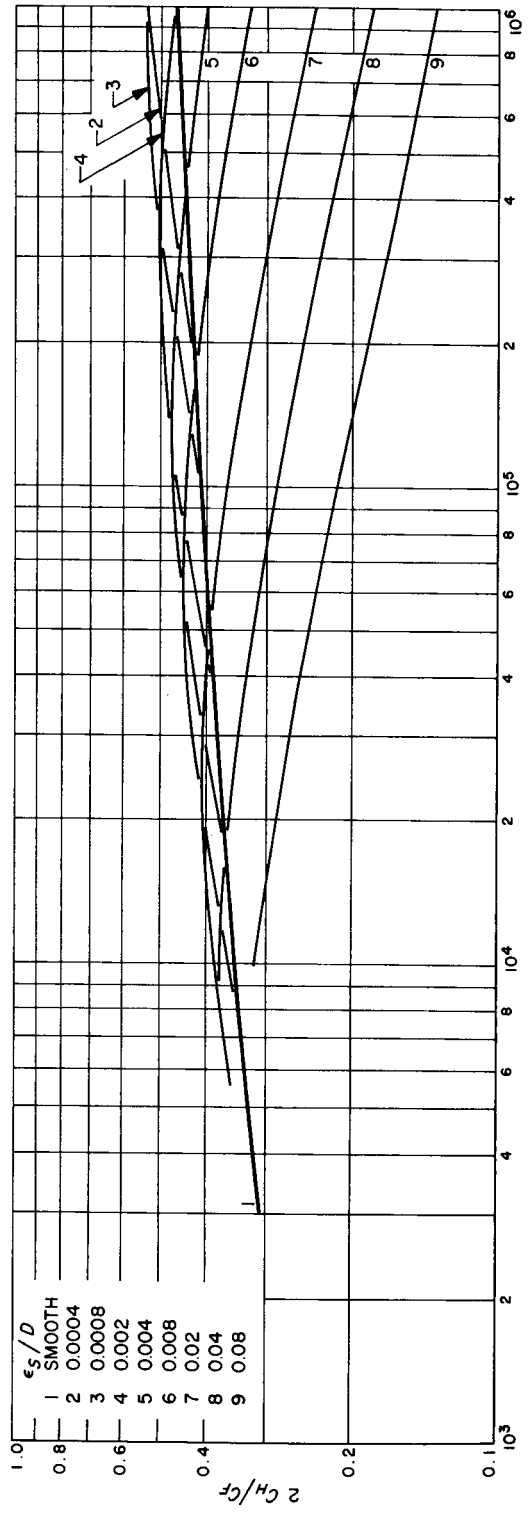

Fig. 19. Comparisons of heat-transfer to friction coefficient ratio vs Reynolds number or $Pr = 6.0$ generated from the similarity functions $g\{\epsilon^*; Pr\}$ and $A\{\epsilon^*\}$

A simple illustration of the possible advantages of employing roughened tubes can be demonstrated as a consequence of items 1 and 4 above. In a heat exchanger designed for water flow through tubes with the controlling thermal resistance on the water side, it would always be possible to replace smooth tubes by selected rough tubes having only one-half of the length of the smooth tubes. This could be done without changing the number of tubes, the tube diameter, the flow rate, the pressure drop, the amount of heat exchanged, the maximum wall temperature, or the temperature difference between the wall and the bulk fluid. Thus, to a first order, the size and weight of the heat exchanger could be reduced by a factor of two without affecting any other system condition.

Finally, in contemplating the use of rough tubes, consideration must be given to the competition between this and other methods of improving heat exchanger efficiency. One such method is the induction of swirl flow in pipes by the use of twisted tapes passing through the pipes. Two of the more favorable swirl flow conditions studied by Gambill, Bundy, and Wansbrough (Ref. 16) were compared with rough tubes having roughness ratios selected to produce the same increase in friction factor. The rough tubes gave nearly the same C_H/C_F performance as that obtained with swirl flow. This suggests that these two methods are indeed competitive means for improving heat exchanger efficiency. This is true at least for operation at low heat flux values.

NOMENCLATURE

A friction similarity function, defined by Eq. (3)

B empirical constant from Eq. (3) and (4)

C_F dimensionless friction coefficient for tubes, $C_F \equiv 2\tau_0/\rho u_m^2$

C_H dimensionless heat transfer coefficient for tubes, $C_H \equiv q_0/\rho u_m c_p(T_w - T_L)$

C_{Hc} roughness-cavity Stanton number, defined by Eq. (17)

c_p specific heat at constant pressure

D tube inside diameter, defined volumetrically for rough tubes

E empirical constant from Eq. (3)

f general function

F function, defined by Eq. (15)

g dimensionless heat transfer similarity function, defined by Eq. (14)

k thermal conductivity

Pr Prandtl number, $Pr \equiv c_p\mu/k$

q_0 mean heat flux normal to the tube wall

r radius coordinate

R tube radius, $R \equiv D/2$

Re Reynolds number for tubes, $Re \equiv Du_m/\nu$

T temperature

T_L mixed-mean fluid temperature

T_w tube wall temperature

u mean axial velocity, a function of y only

u_m tube discharge velocity, $u_m \equiv (2/R^2)\int_0^R u\{r\}\, r\, dr$

u_τ friction velocity, $u_\tau \equiv (\tau_0/\rho)^{1/2}$

w mass flow rate

x axial distance coordinate, originates at the start of heating

y distance from the wall coordinate

y^* dimensionless distance from the wall, $y^* \equiv yu_\tau/\nu$

ΔP_{TS} pressure-drop in the test section

ΔT_f temperature difference between the wall and the local mixed-mean fluid, $\Delta T_f \equiv T_w - T_L$

ε roughness height

ε_m turbulent diffusion coefficient for momentum transfer

ε_h turbulent diffusion coefficient for heat transfer

ε_s sand-grain roughness height for equivalent friction coefficient at fully rough conditions

ε^* dimensionless roughness height, $\varepsilon^* \equiv \varepsilon u_\tau/\nu$

μ absolute viscosity

ν kinematic viscosity

ρ density

τ_0 mean shear stress at the tube wall

{ } braces are used exclusively as a functional form, e.g., $f\{Re; Pr\}$ is read, "the variable f, a function of Re with Pr as a parameter."

Subscripts

FR fully rough

g average value on that surface described by the tips of the roughness elements

S smooth

REFERENCES

1. Nikuradse, J., "Laws for Flow in Rough Pipes," *VDI-Forschungsheft* 361, Series B, Vol. 4 (1933); Translation, Brielmaier, A. A., *NACA TM 1292* (1950).

2. Cope, W. F., "The Friction and Heat Transmission Coefficients of Rough Pipes," *Proceedings of the Institute of Mechanical Engineers,* Vol. 145 (1941), pp. 99–105.

3. Nunner, W., "Heat Transfer and Pressure Drop in Rough Tubes," *VDI-Forschungsheft 455,* Series B, Vol. 22 (1956), pp. 5–39; *A.E.R.E. Lib./Trans. 786* (1958) by F. Hudswell.

4. Dipprey, D. F., "An Experimental Investigation of Heat and Momentum Transfer in Smooth and Rough Tubes at Various Prandtl Numbers," Ph. D. Thesis, California Institute of Technology (1961).

5. Allen, R. W., "Measurements of Friction and Local Heat Transfer for Turbulent Flow of a Variable Property Fluid (Water) in a Uniformly Heated Tube," Ph. D Thesis, University of Minnesota (September 1959).

6. Eagle, A. and R. M. Ferguson, "On the Coefficient of Heat Transfer from the Internal Surface of Tube Walls," *Proceedings of the Royal Society,* Vol. 127 (June, 1930), pp. 540–566.

7. Rannie, W. D., "Heat Transfer in Turbulent Shear Flow," Ph. D. Thesis, California Institute of Technology (1951); also *Journal of the Aeronautical Sciences,* Vol. 23 (May 1956), pp. 485–489.

8. Townsend, A. A., *The Structure of Turbulent Shear Flow,* University Press, Cambridge (1956).

9. von Kármán, T., "The Analogy between Fluid Friction and Heat Transfer," *Transactions of the ASME,* Vol. 61 (1939), pp. 705–710.

10. Deissler, R. G., "Analysis of Turbulent Heat Transfer, Mass Transfer, and Friction in Smooth Tubes at High Prandtl and Schmidt Numbers," *NACA Report 1210* (1955).

11. Wieghardt, K., "Erhöhung des turbulenten Reibungswiderstandes durch Oberflächenstörungen (Increase of the Turbulent Frictional Resistance Caused by Surface Irregularities)," Forschungsbericht 1563, ZWB, (March, 1942); also, *Jahrb, deutchen Luftfhartforschung* (1943), pp. 1–17.

12. Smith, J. W. and N. Epstein, "Effect of Wall Roughness on Convective Heat Transfer in Commercial Pipes," Journal of the American Institute of Chemical Engineers, Vol. 3 (June, 1957), pp. 242–248.

13. Fortescue, P. and W. B. Hall, "Heat Transfer Experiments on the Fuel Elements," *Journal of British Nuclear Energy Conference,* Vol. 2, No. 2 (April, 1957), p. 83.

14. Grass, G., "The Improvement of Heat Transfer to Water Derivable from the Artificial Roughening of Surfaces in Reactors or in Heat Exchangers," *Atomkernenergie,* Vol. 3 (1958), pp. 328–331; *AEC Translation No. 3641* by G. Dessauer.

15. Martinelli, R. C., "Heat Transfer to Molten Metals," *Translations of the ASME,* Vol. 69 (1947), p. 947.

16. Gambill, W. R., R. D. Bundy, and R. W. Wansbrough, "Heat Transfer Burnout, and Pressure Drop for Water in Swirl Flow through Tubes with Internal Twisted Tapes," Oak Ridge National Laboratory, No. 2911 (March, 1960).

17. Schlichting, H., *Boundary Layer Theory,* McGraw-Hill, New York (1955).